TWO-DIMENSIONAL ELECTRONS, HOLES, MAGNETOEXCITONS, AND CAVITY POLARITONS UNDER THE ACTION OF STRONG PERPENDICULAR MAGNETIC AND ELECTRIC FIELDS

I. V. Podlesny

Institute of Applied Physics, Academy of Sciences of Moldova, str. Academiei 5, Chisinau, MD-2028 Republic of Moldova

(Received April 11, 2017)

Abstract

The review is focused on the energy spectrum of two-dimensional electrons, holes, magnetoexcitons, and cavity polaritons under the action of strong magnetic and electric fields perpendicular to the surface of GaAs-type quantum wells (QWs) with a *p*-type valence band embedded into resonators. As the first step in this direction, the Landau quantization (LQ) of electrons and heavy holes (hhs) has been studied taking into account the Rashba spin-orbit coupling (RSOC) with third-order chirality terms for hhs and nonparabolicity terms in their dispersion law, including the Zeeman splitting (ZS) effects. The nonparabolicity terms proportional to the electric field strength have been introduced to avoid the collapse of the semiconductor energy gap under the action of the third-order chirality terms. Exact solutions for the eigenfunctions and eigenenergies for the LQ task have been obtained on the basis of the Rashba method [1]. In the next steps of our review paper, we have deduced Hamiltonians describing the Coulomb electron–electron and electron–radiation interactions in the second quantization representation. They make it possible to determine the magnetoexciton energy branches and deduce the Hamiltonian of the magnetoexciton–photon interaction. The fifth-order dispersion equation describing the energy spectrum of the cavity magnetoexciton–polaritons has been studied. It takes into account the interaction of the cavity photons with two dipole-active and two quadrupole-active 2D magnetoexciton energy branches. The cavity photons have circular polarizations $\vec{\sigma}_{\vec{k}}^{\pm}$ oriented along their wave vectors $\vec{k}$ with quantized longitudinal components $k_z = \pm\pi/L_c$, where L_c is the resonator length, and with small transverse components $\vec{k}_{\parallel}$ oriented in the plane of the QW. The 2D magnetoexcitons are characterized by in-plane wave vectors $\vec{k}_{\parallel}$ and circular polarizations $\vec{\sigma}_M$ arising in the *p*-type valence band with magnetic momentum projection $M = \pm 1$ in the direction of the magnetic field. The selection rules of the exciton–photon interaction have two origins. One of them, of geometrical type, is expressed in terms of the scalar products of the two types of circular polarizations. They depend on in-plane wave vectors $\vec{k}_{\parallel}$ even in the case of dipole-active transitions, because the cavity photons have an oblique incidence to the surface of the QW. The other origin is related with numbers n_e and n_h of the LQ levels of electrons and hhs involved in the magnetoexciton formation. Thus, the dipole-active transitions take place under condition $n_e = n_h$, whereas in the quadrupole-active transitions the relationship is as follows: $n_e = n_h \pm 1$. The optical gyrotropy effects appear changing the sign of the photon circular polarization at a given sign of wave vector longitudinal projection k_z or

equivalently changing the sign of longitudinal projection k_z at the same selected circular polarization of light.

1. Introduction

The authors of [1–4] proposed a theoretical description of the electron structure of magnetoexcitons and the excitonic spectra in GaN-based quantum wells (QWs) in a wide range of perpendicular magnetic fields up to 60 T. The built-in strain and perpendicular electric field were taken into account. The pressure leads to the reordering of the topmost valence subbands having different symmetries. The exciton binding energies at different valence subbands give rise to the reordering of the respective optical transitions in the emission and absorption spectra. The reordering in the light- and heavy-hole (hh) valence subbands takes place also in dependence on the QW width. The latter is an important feature of GaN-type semiconductors; it leads to a step-like dependence of the excitonic *g*-factor. An electric field perpendicular to the layer surface was taken into account together with the size quantization; it determines the electron and hole orbital wave functions in this direction. The Landau orbitals in [2, 3] were generated by the ladder operators constructed using the Lamb gauge transformation [5]. They concern only the states with a zero center-of-mass momentum, depend on coordinates of the relative electron–hole motion, and act on the ground state wave function with the same coordinate dependence.

In contrast to this model, below, we will consider a two-dimensional (2D) electron–hole (e–h) system in a GaAs-type structure with only one hh valence subband with infinitesimal QW width without any reference to the excited levels of the size quantization. Instead, we will consider the multilateral phenomena related to Landau quantization (LQ) accompanied by the Rashba spin–orbit coupling (RSOC), Zeeman splitting (ZS), and nonparabolicity (NP) of the hh dispersion law. All of them are induced in the 2D e–h system by the action of the strong perpendicular magnetic and electric fields. Our results were obtained following the Rashba's basic paper [1] using the rising and the lowering operators in the space of the single-particle Landau levels. In the case of [6–9] they depend exclusively on the electron and hole coordinates, avoiding their expressing through the relative and center-of-mass coordinates of the e–h pair. The respective functions were determined by the exact solutions [6, 7]. The magnetoexciton wave function in coordinate representation when the electron and hole are situated on the lowest Landau levels (LLLs) was deduced in [8, 9]. It represents the interdependence of the translational and relative electron and hole motions in the presence of a magnetic field.

The research of the magnetic factors and ZS of electrons, holes, and excitons in QWs is significant because it gives insight into the subband structure and the coupling between exciton states. The ZS shows the inversion of sign and nonlinear variation [10] associated with level crossing (or anticrossing) among the excitonic states at different magnetic fields. The effects of size quantization considerably influence the value of electron *g*-factor in the semiconductor structures with QWs. Due to these effects, the electron *g*-factor becomes anisotropic and depends on well width [11] and layers thickness of the heterostructure [12].

The hhs also have a strongly anisotropic *g*-factor [13, 14]. According to [15], the exciton recombination dynamics in a magnetic field is determined, being governed by the fine structure of the exciton states splitted by the magnetic field, and the splittings are determined by the signs and magnitudes of the electron [16, 17] and hh Lande *g*-factors. The value of the hole *g*-factor in GaAs/AlAs QW samples is determined by the mixing of heavy and light hole bands. Therefore, it is very sensitive to the QW thickness and interface roughness and could be large and positive [18–20].

The different cases of positive and negative electron and hole *g*-factors are considered in our review paper to demonstrate the contributions at high magnetic fields of the ZSs to the magnetoexciton and polariton energies.

In recent years, much attention has been paid to the magnetic field effect on microcavity polaritons [21–25]. The rich variety of nonlinear effects induced by a magnetic field includes the suppression of polariton superfluidity and the density-dependent ZS [23, 25]. The authors of [21, 22] experimentally observed the transverse electric–transverse magnetic (TE–TM) splitting of the cavity modes, the Faraday rotation of the plane polarization of the light passing through the microcavity, and the ZS of the exciton eigenstates.

The magnetic field was used as a tuning parameter for exciton and photon resonances [26]. In this way, the change in the exciton energy, the oscillator strength, the polariton line width, and the redistribution of the polariton density along the dispersion curve were obtained. All of them are due to the magnetically induced detuning [26]. The experimentally observed increase in the exciton oscillator strength as a function of magnetic field strength B [26] is in qualitative accordance with the theoretical result of [27], where Rabi frequency Ω_R of the magnetoexciton polariton is inversely proportional to magnetic length l_0 as follows: $\Omega_R \sim l_0^{-1} \sim \sqrt{B}$. This means that, in this case, the oscillator strength is proportional to B. The evolution of the circularly polarized nonequilibrium Bose–Einstein condensates of the spinor–polaritons in different spinor states [24] and the effect of the magnetic field on a spinor exciton polariton condensate in rectangular GaAs microcavity pillars [28] were investigated. The authors of [29] studied the ZS and the diamagnetic shift of the exciton–polariton energy spectrum in an external magnetic field for different trap diameters. The new Hopfield coefficients [30] in the presence of a magnetic field and the effect of the relative weights of the photonic and excitonic components in the structure of the polariton branches were determined in [31]. The combined exciton–cyclotron resonance in GaAs-type QWs was revealed experimentally [32] and explained theoretically [33].

Our review paper is organized as follows. In Section 2, the wave functions and the eigenenergies of the 2D electrons and hhs undergoing the LQ, RSOC, and ZS effects are deduced. Section 3 is dedicated to the description of the electron–electron Coulomb interaction under these conditions determining the properties of the magnetoexcitons. The electron-radiation interaction, the magnetoexciton–photon coupling, and the formation of the magnetoexciton–polaritons are studied in Section 4. Conclusions are made in Section 5.

2. 2D Electrons and Holes Under the Action of Perpendicular Magnetic and Electric Fields

The Hamiltonians describing the LQ, RSOC, and Zeeman effect involving 2D electrons and holes were deduced in [1, 6, 7, 34–36]. They are as follows:

$$H_e = \hbar\omega_{ce}\left\{\left(a^+a+\frac{1}{2}\right)\hat{I} + i\sqrt{2}\alpha\begin{vmatrix} 0 & a \\ -a^+ & 0 \end{vmatrix} + Z_e\hat{\sigma}_z\right\},$$

$$H_h = \hbar\omega_{ch}\left\{\left[\left(a^+a+\frac{1}{2}\right)+\delta\left(a^+a+\frac{1}{2}\right)^2\right]\hat{I} + i2\sqrt{2}\beta\begin{vmatrix} 0 & \left(a^+\right)^3 \\ -\left(a\right)^3 & 0 \end{vmatrix} - Z_n\hat{\sigma}_z\right\}. \quad (1)$$

Here, Bose-type operators a^{+}, a generating Fock states $|m\rangle$ were introduced; the following notations were used [37–39]:

$$Z_i = \frac{g_i \mu_B B}{2\hbar\omega_{ci}} = \frac{g_i m_i}{4m_0},\ \omega_{ci} = \frac{eB}{m_i c},\ i = e,h,\ \hat{I} = \begin{vmatrix} 1 & 0 \\ 0 & 1 \end{vmatrix},\ \hat{\sigma}_z = \begin{vmatrix} 1 & 0 \\ 0 & -1 \end{vmatrix},\ \mu_B = \frac{e\hbar}{2m_0 c},\ e = |e| > 0,$$
$$B = y\ \mathrm{T},\ E_z = x\,\frac{\mathrm{kV}}{\mathrm{cm}},\ \alpha = 8\cdot 10^{-3}\, x/\sqrt{y},\ \beta = 1.06\cdot 10^{-2}\, x\sqrt{y},\ \delta = 10^{-4} Cxy, \tag{2}$$

where ω_{ci} are the cyclotron frequencies, Z_i are the Zeeman parameters proportional to g-factors g_i and to effective masses m_i of the electrons and holes, whereas m_0 is the bare electron mass; δ is the NP of the hh dispersion law; α and β are the parameters of the chirality terms, which are of the first order in the case of the electrons [1] and of the third order in the case of the hhs [37–39].

The solutions of these equations were chosen in the dimensionless forms. For the case of electrons, we have

$$\mathsf{H}_e = \frac{H_e}{\hbar\omega_{ce}};\ \mathsf{H}_e|\psi_e\rangle = \varepsilon|\psi_e\rangle;\ |\psi_e\rangle = \begin{vmatrix} |f_1\rangle \\ |f_2\rangle \end{vmatrix},$$
$$|f_1\rangle = \sum_n a_n|n\rangle;\ |f_2\rangle = \sum_n b_n|n\rangle;\ \sum_n |a_n|^2 + \sum_n |b_n|^2 = 1. \tag{3}$$

The two equations that determine coefficients a_n and b_n are as follows [1]:

$$\sum_{n\geq 0} a_n\left[n + \frac{1}{2} + Z_e - \varepsilon\right]|n\rangle = -i\sqrt{2}\alpha\sum_{n\geq 1} b_n\sqrt{n}\,|n-1\rangle$$
$$\sum_{n\geq 0} b_n\left[n + \frac{1}{2} - Z_e - \varepsilon\right]|n\rangle = i\sqrt{2}\alpha\sum_{n\geq 0} a_n\sqrt{n+1}\,|n+1\rangle. \tag{4}$$

They lead to the equations for coefficients a_m and b_m at $m \geq 0$. Based on them, we obtain the equalities

$$\varepsilon_m^{\pm} = (m+1) \pm \sqrt{\left(\frac{1}{2} - Z_e\right)^2 + 2|\alpha|^2(m+1)},$$
$$|a_m^-|^2 = \frac{\left[\left(\frac{1}{2} - Z_e\right) + \sqrt{\left(\frac{1}{2} - Z_e\right)^2 + 2|\alpha|^2(m+1)}\right]^2}{\left[\left(\frac{1}{2} - Z_e\right) + \sqrt{\left(\frac{1}{2} - Z_e\right)^2 + 2|\alpha|^2(m+1)}\right]^2 + 2|\alpha|^2(m+1)}, \tag{5}$$
$$|a_m^{\pm}|^2 = |b_{m+1}^{\mp}|^2;\ |a_m^{\pm}|^2 + |b_{m+1}^{\pm}|^2 = 1;\ m \geq 0.$$

The wave function in the second quantization representation has the form

$$|\psi_m^{\pm}\rangle = \begin{vmatrix} a_m^{\pm}|m\rangle \\ b_{m+1}^{\pm}|m+1\rangle \end{vmatrix};\ \ \langle\psi_m^{\pm}| = \left|(a_m^{\pm})^*\langle m| \quad (b_{m+1}^{\pm})^*\langle m+1|\right| \tag{6}$$

and obey to the orthogonality condition

$$\left\langle \psi_m^+ \middle| \psi_m^- \right\rangle = \left(a_m^+\right)^* a_m^- + \left(b_{m+1}^+\right)^* b_{m+1}^- = 0.$$

In the coordinate representation, the wave functions are

$$\left|\psi_m^{\pm}(\vec{r})\right\rangle = \frac{e^{ipx}}{\sqrt{L_x}} \begin{vmatrix} a_m^{\pm}\varphi_m(\eta) \\ b_{m+1}^{\pm}\varphi_{m+1}(\eta) \end{vmatrix}; \;\; \eta = \frac{y}{l} - pl, \tag{7}$$

where L_x is the length of the layer. These states have been first obtained by Rashba [1] and are repeated here including Zeeman coefficient Z_e.

Side by side with the solutions $\left|\psi_m^{\pm}\right\rangle$ at $m \ge 0$, there also exists one solution with $b_0 = 1$ of the type

$$\varepsilon_0 = \frac{1}{2} - Z_e; \;\; \left|\psi_0\right\rangle = \begin{vmatrix} 0 \\ |0\rangle \end{vmatrix}; \;\; \left|\psi_0(\vec{r})\right\rangle = \frac{e^{ipx}}{\sqrt{L_x}} \begin{vmatrix} 0 \\ \varphi_0(\eta) \end{vmatrix}, \tag{8}$$

which is orthogonal to any solutions (6).

In terms of energy units, the energy spectrum is

$$E_m^{\pm} = \hbar\omega_{ce}\varepsilon_m^{\pm}, \, m \ge 0; \;\; E_0 = \hbar\omega_{ce}\varepsilon_0. \tag{9}$$

Below, we will consider only two LLLs for conduction electrons, namely, state $\left|\psi_0^-\right\rangle$ (7) and $\left|\psi_0\right\rangle$ (8). They will be denoted as (eR_1) and (eR_2), respectively. In Fig. 1, the dependences of the energy levels $E_0^{\pm}(B)$ and $E_0(B)$ on magnetic field strength *B* are denoted by levels $0^{\pm}$ and 0, respectively. The two lowest energy levels 0^- and 0 change their positions on the energy scale as a function of the values of electron *g*-factor g_e.

The hh Hamiltonian in dimensionless form has the form

$$\mathsf{H} = \frac{H_h}{\hbar\omega_{ch}} = \left\{ \left[\left(a^+a + \frac{1}{2}\right) + \delta\left(a^+a + \frac{1}{2}\right)^2 \right]\hat{I} + i2\sqrt{2}\beta + \begin{vmatrix} 0 & \left(a^+\right)^3 \\ -(a)^3 & 0 \end{vmatrix} - Z_h\hat{\sigma}_z \right\};$$

$$\mathsf{H}\left|\psi\right\rangle = \varepsilon\left|\psi\right\rangle \tag{10}$$

$$\left|\psi\right\rangle = \begin{vmatrix} |f_1\rangle \\ |f_2\rangle \end{vmatrix}; \;\; |f_1\rangle = \sum_{n\ge 0} c_n |n\rangle; \;\; |f_2\rangle = \sum_{n\ge 0} d_n |n\rangle.$$

Using the properties of the Fock states

$$\underset{n\ge 3}{a^3|n\rangle = \sqrt{n(n-1)(n-2)}\,|n-3\rangle}; \;\; \underset{n\ge 0}{\left(a^+\right)^3|n\rangle = \sqrt{(n+1)(n+2)(n+3)}\,|n+3\rangle} \tag{11}$$

one can transcribe Pauli equation (11) in the form of two algebraic equations

$$\begin{aligned} &\sum_{n\ge 0} c_n \left[\left(n + \frac{1}{2}\right) + \delta\left(n + \frac{1}{2}\right)^2 - Z_h - \varepsilon \right] |n\rangle = -i2\sqrt{2}\beta \sum_{n\ge 0} d_n \sqrt{(n+1)(n+2)(n+3)}\,|n+3\rangle \\ &\sum_{n\ge 0} d_n \left[\left(n + \frac{1}{2}\right) + \delta\left(n + \frac{1}{2}\right)^2 + Z_h - \varepsilon \right] |n\rangle = i2\sqrt{2}\beta \sum_{n\ge 3} c_n \sqrt{n(n-1)(n-2)}\,|n-3\rangle. \end{aligned} \tag{12}$$

After some transformations of equations (12), we will obtain two linear algebraic equations determining coefficients c_m and d_{m-3} at $m \geq 3$. They determine the energy spectrum as follows:

$$\varepsilon_m^{\pm} = \frac{E_m^{\pm}}{\hbar\omega_{ch}} = (m-1) + \delta\left(m^2 - 2m + \frac{13}{4}\right) \pm \sqrt{\left[\frac{3}{2} - Z_h + 3\delta(m-1)\right]^2 + 8\beta^2 m(m-1)(m-2)}, \quad (13)$$

$m \geq 3.$

Coefficients $c_m^{\pm}$, $d_{m-3}^{\pm}$ at $m \geq 3$ have the form

$$c_m^{-} = \frac{-i2\sqrt{2}\beta\sqrt{m(m-1)(m-2)}\,d_{m-3}^{-}}{\left[\frac{3}{2} - Z_h + 3\delta(m-1) + \sqrt{\left[\frac{3}{2} - Z_h + 3\delta(m-1)\right]^2 + 8\beta^2 m(m-1)(m-2)}\right]},$$

$$d_{m-3}^{+} = \frac{-i2\sqrt{2}\beta\sqrt{m(m-1)(m-2)}\,c_m^{+}}{\left[\frac{3}{2} - Z_h + 3\delta(m-1) + \sqrt{\left[\frac{3}{2} - Z_h + 3\delta(m-1)\right]^2 + 8\beta^2 m(m-1)(m-2)}\right]}, \quad (14)$$

$$\left|c_m^{+}\right|^2 = \left|d_{m-3}^{-}\right|^2, \ \left|c_m^{-}\right|^2 = \left|d_{m-3}^{+}\right|^2, \ m \geq 3.$$

The respective wave functions have the form

$$\left|\psi_m^{\pm}\right\rangle = \begin{vmatrix} c_m^{\pm}\left|m\right\rangle \\ d_{m-3}^{\pm}\left|m-3\right\rangle \end{vmatrix}, \quad \left|\psi_m^{\pm}(\vec{r})\right\rangle = \frac{e^{iqx}}{\sqrt{L_x}}\begin{vmatrix} c_m^{\pm}\varphi_m(\eta) \\ d_{m-3}^{\pm}\varphi_{m-3}(\eta) \end{vmatrix}, \quad \eta = \frac{y}{l} + ql. \quad (15)$$

They obey to the normalization and orthogonality conditions

$$\left\langle\psi_m^{\pm}\middle|\psi_m^{\pm}\right\rangle = \left|c_m^{\pm}\right|^2 + \left|d_{m-3}^{\pm}\right| = 1, \ \left\langle\psi_m^{+}\middle|\psi_m^{-}\right\rangle = c_m^{+*}c_m^{-} + d_{m-3}^{+*}d_{m-3}^{-} = 0. \quad (16)$$

Side by side with solutions (15), there are three other solutions at $m = 0,1,2.$ They are as follows:

$$\begin{aligned} &c_0 = 1, \ \left|\psi_0\right\rangle = \begin{vmatrix} \left|0\right\rangle \\ 0 \end{vmatrix}, \ \left|\psi_0(\vec{r})\right\rangle = \frac{e^{iqx}}{\sqrt{L_x}}\begin{vmatrix} \varphi_0(\eta) \\ 0 \end{vmatrix}, \quad \varepsilon_0 = \frac{1}{2} + \frac{\delta}{4} - Z_h, \\ &c_1 = 1, \ \left|\psi_1\right\rangle = \begin{vmatrix} \left|1\right\rangle \\ 0 \end{vmatrix}, \ \left|\psi_1(\vec{r})\right\rangle = \frac{e^{iqx}}{\sqrt{L_x}}\begin{vmatrix} \varphi_1(\eta) \\ 0 \end{vmatrix}, \quad \varepsilon_1 = \frac{3}{2} + \frac{9}{4}\delta - Z_h, \\ &c_2 = 1, \ \left|\psi_2\right\rangle = \begin{vmatrix} \left|2\right\rangle \\ 0 \end{vmatrix}, \ \left|\psi_2(\vec{r})\right\rangle = \frac{e^{iqx}}{\sqrt{L_x}}\begin{vmatrix} \varphi_2(\eta) \\ 0 \end{vmatrix}, \quad \varepsilon_2 = \frac{5}{2} + \frac{25}{4}\delta - Z_h. \end{aligned} \quad (17)$$

All of them are orthogonal to previous solutions (15).

Figure 2 represents hh energy levels $E_h^{-}(3)$ for different values of the *g*-factor and magnetic field strength *B*, and parameters *C* and *x*. The magnetoexcitons in GaAs-type crystals are formed at a magnetic field strength of $B \geq 10$ T. The lowest of levels $E_h^{\pm}(m)$ with $m = 3,4,\ldots,10$ and $E_h(m)$ with $m = 0,1,2$ are $E_h^{-}(3)$, $E_h(0)$ and $E_h^{-}(4)$.

The LQ and the energy levels of the electrons and holes determine the energies of the optical band-to-band quantum transitions and the magnetoexciton creation energy.

The band-to-band quantum transitions can be discussed in a more large range of parameters because they do not need the knowledge about the ionization potentials of the magnetoexcitons. The quantum transitions from the ground state of the crystal to the magnetoexciton states and to the states of an electron–hole (e–h) pair without Coulomb e–h interaction will be considered taking into account three LLLs for holes denoted as (h, R_j) with $j = 1, 2, 3$ and two LLLs for electrons denoted as (e, R_i) with $i = 1,2$. These combinations have the energies of the band-to-band transitions $E_{cv}(F_n)$. Being accounted from the semiconductor energy band gap E_g^0, they are as follows:

$$E_{cv}(F_n) - E_g^0 = E_e(R_i) + E_h(R_j). \tag{18}$$

They are represented in Figs. 3 and 4 in dependences on magnetic field strength B and on g-factors g_e and g_h at different parameters of the RSOC and the nonparabolic hh dispersion law.

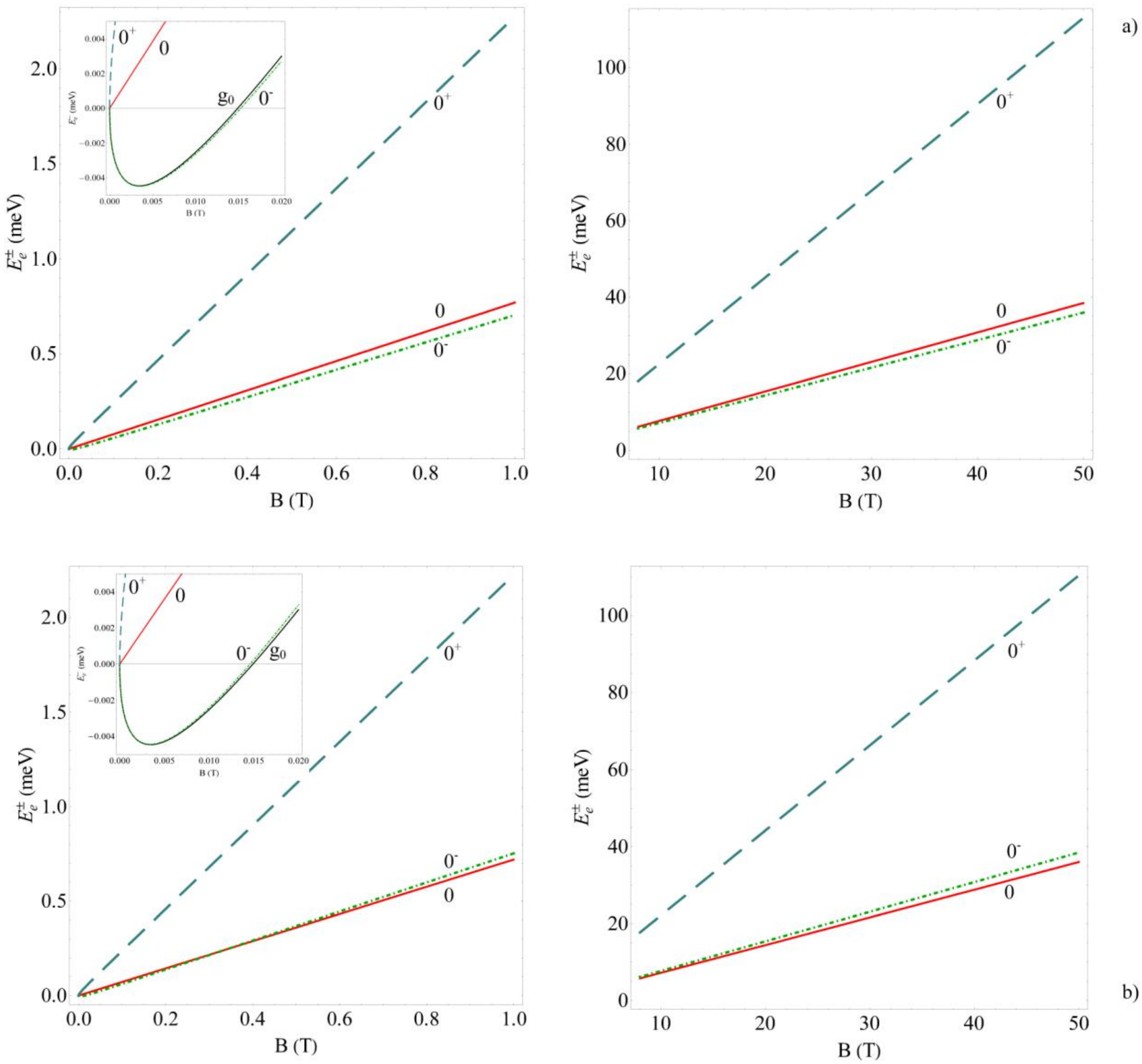

Fig. 1. Electron branches of LQ levels $E_e^{\pm}(0)$ and $E_e(0)$ for parameter x =10 and two different values of g-factor: (a) g_e= –1 and (b) g_e= –1. In the inset, the case of zero value for the electron g-factor is denoted by the g_0 curve.

Figure 3 shows only the effect of the LQ and the ZS under the action of a perpendicular magnetic field. In this case, we have parameters $x = 0$ and $C = 0$. In the presence of a supplementary electric field with the same direction, an additional RSOC takes place being accompanied by the NP of the hh dispersion law induced also by the electric field. The effect of these four factors, namely of LC, ZS, RSOC, and NP, is represented in Fig. 4 for some particular parameters.

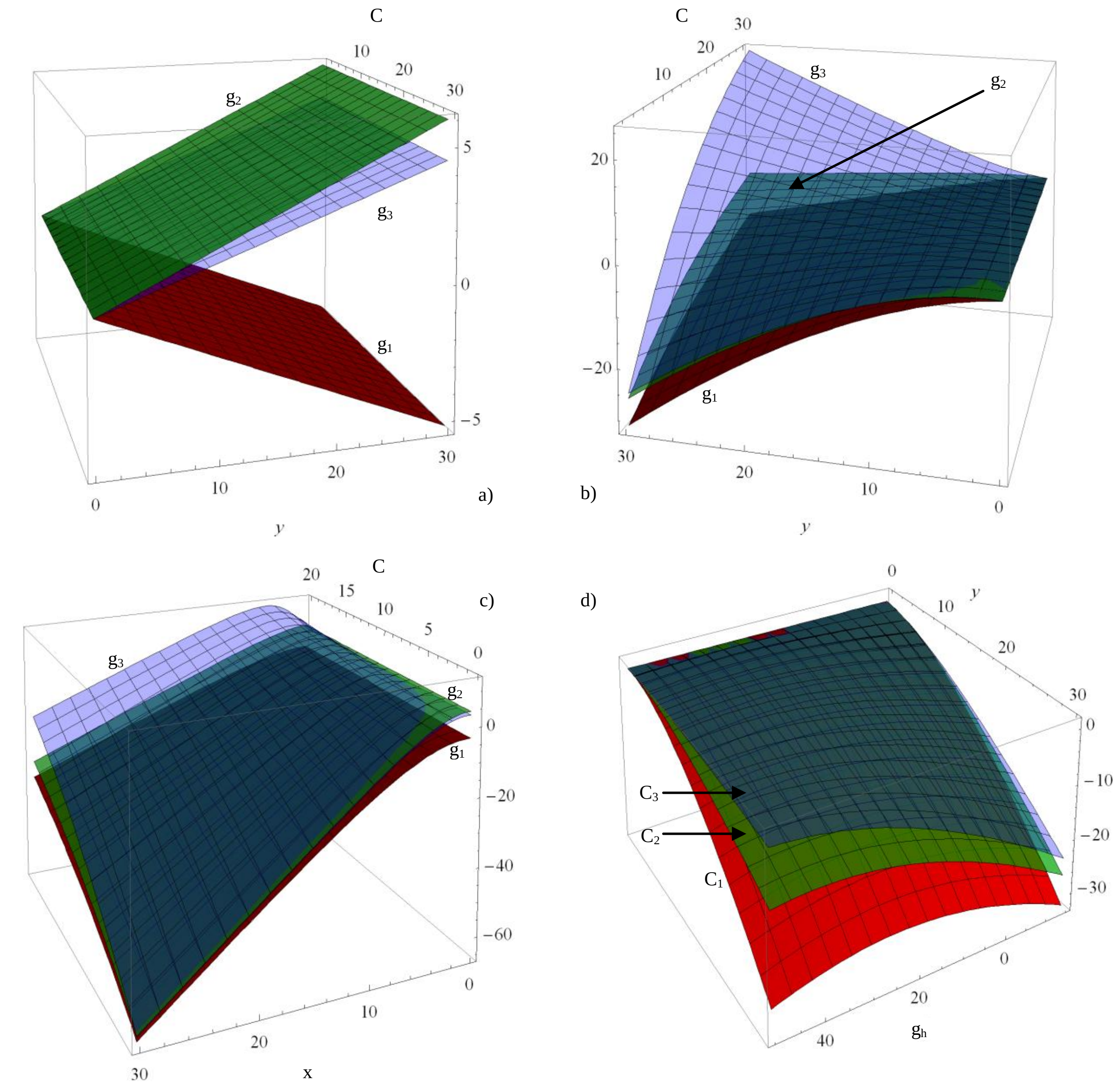

Fig. 2. Heavy hole LQ levels $E_h^-(m, C, x, y)$, with m = 3 and three values of the g-factor: $g_h = -15$ (g_1), 0 (g_2), and 50 (g_3). The following parameters are selected: (a) x=0; (b) x=10; (c) y=20 T; and (d) C_1=0, C_2=5.8, C_3=10, x=10.

3. Coulomb Electron–Electron Interaction [40, 41] and Magnetoexcitons

Three LLLs for 2D hhs (h,R_j) with $j=1,2,3$ were combined with two LLLs for 2D conduction electrons (e,R_i) with $i=1,2$ giving rise to six 2D magnetoexciton states F_n with $n=1,2...6$ [34–36]. To calculate their ionization potentials, the Hamiltonian of the Coulomb electron–electron interaction under conditions of LQ, RSOC, and ZS is required. It was deduced by the authors of [34–36] taking into account only the first two conditions, namely, LQ and RSOC.

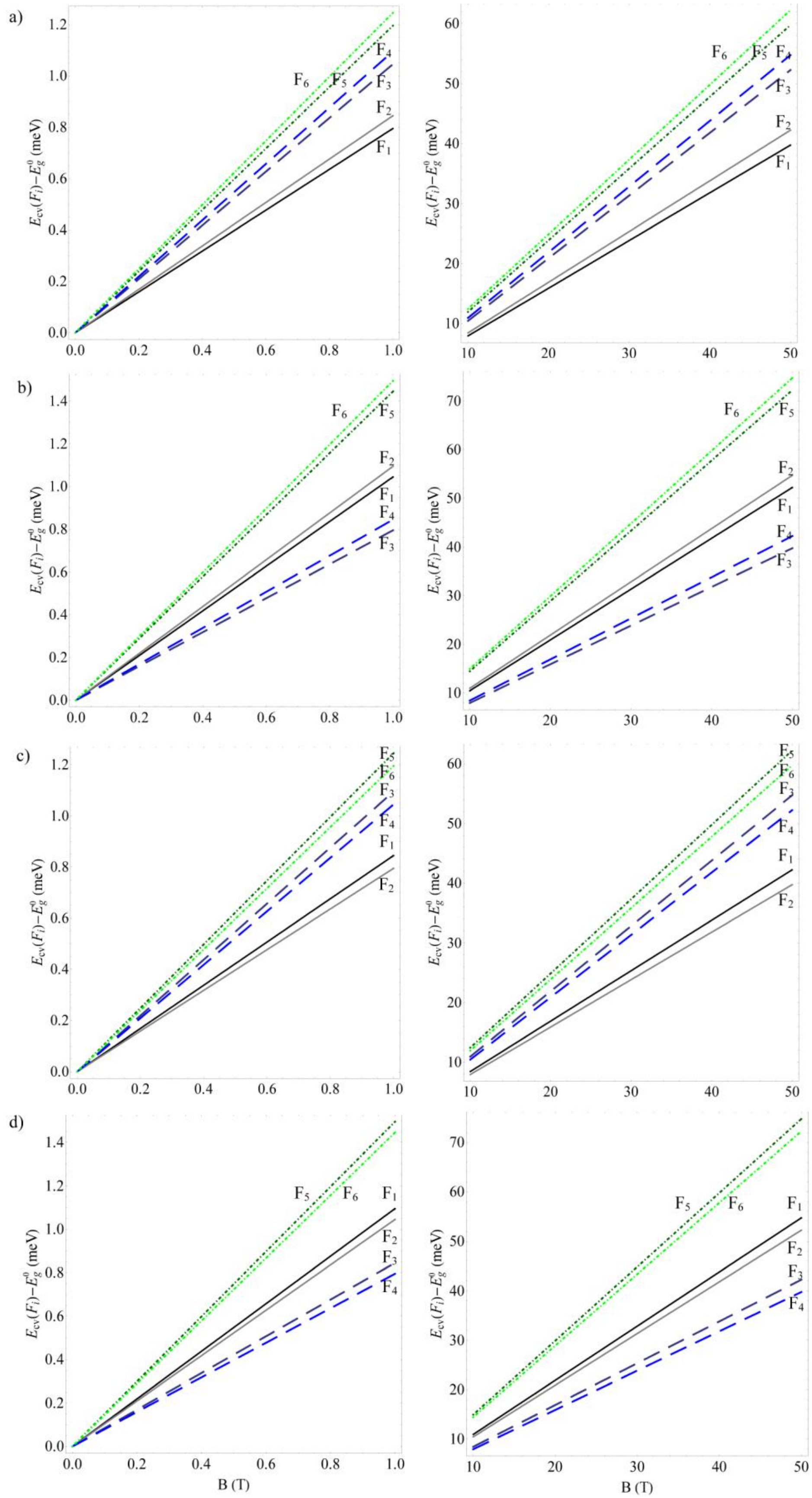

Fig. 3. *Reproduced, with permission, from* [40]: band-to-band quantum transitions energies $E_{cv}\left(F_i\right)-E_g^0$ for six combinations F_i of three hh and of two electron LLLs as a function of magnetic field strength B at different combinations of electron and hhs g_e and g_h: (a) $g_e=-1$, $g_h=-5$; (b) $g_e=-1$, $g_h=5$; (c) $g_e=1$, $g_h=-5$; and (d) $g_e=1$, $g_h=5$. The absence of an electric field leads to the parameters: $x=0$ and $C=0$.

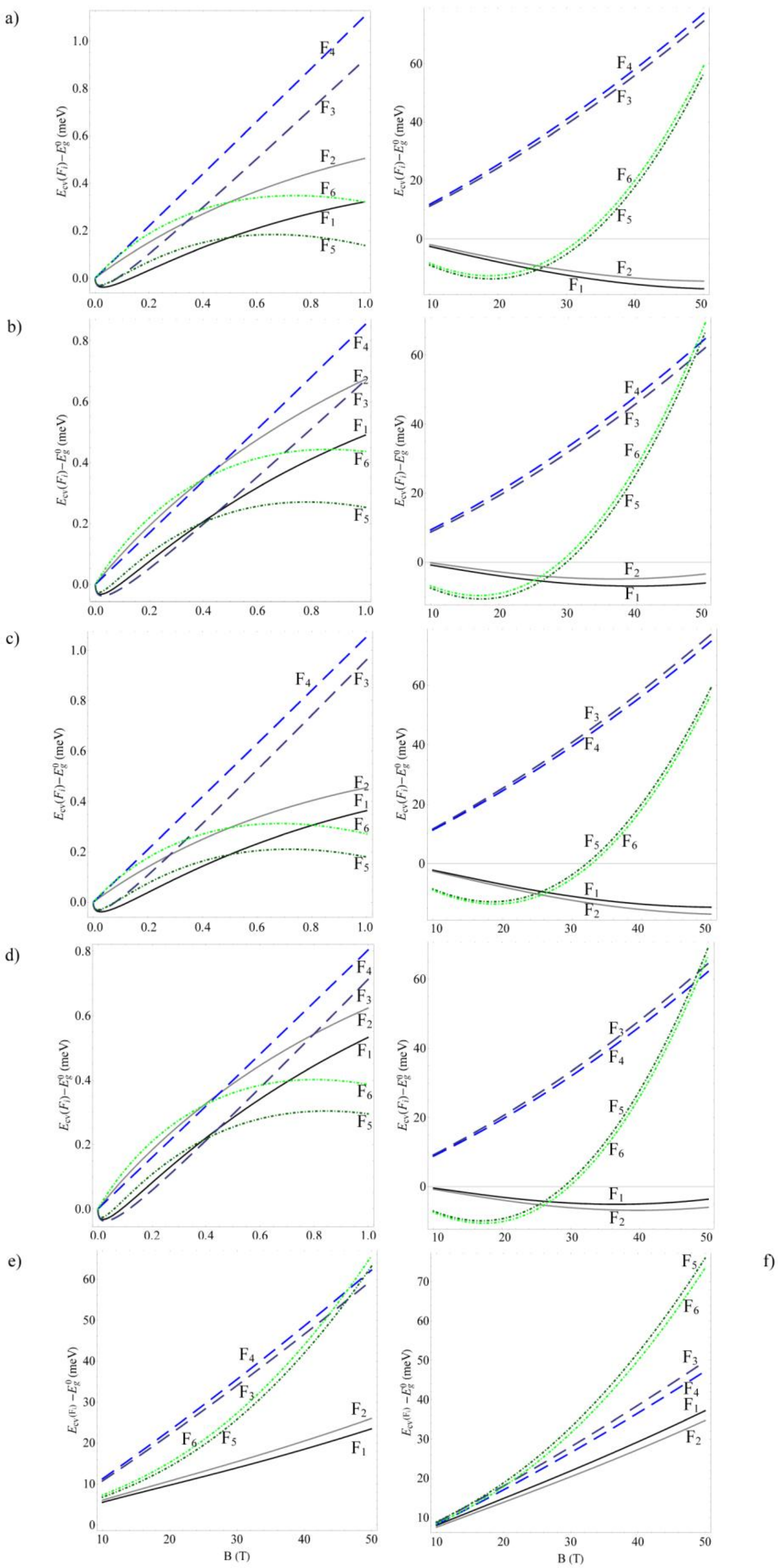

Fig. 4. Band-to-band quantum transitions energies $E_{cv}\left(F_i\right)-E_g^0$ for six combinations F_i of three hh and two electron LLLs as a function of magnetic field strength B at different combinations of the electron and hh g-factors g_e and g_h: (a) g_e = –1, g_h = –5; (b) g_e = –1, g_h = 5; (c) g_e = 1, g_h = –5; and (d) g_e = 1, g_h = 5. The action of the electric field is taken into account choosing the parameters: $x=30$ and $C=30$. Figures 4a–4d are reproduced, with permission, from [40]. The case of the energies with the parameters x = 10 and C = 30 is shown in (e) g_e = –1, g_h = –5 and (f) g_e= 1, g_h = 5.

Below, we will generalize those results adding also the third condition, namely, the ZS effects. The more so, it can be done because the Pauli Hamiltonians containing the Zeeman effects are represented by operators $\pm g_i(\mu_B B/2)\hat{\sigma}_z$, where $\hat{\sigma}_z$ has only diagonal matrix elements. For the e–h pair in the particular combination $\left(R_i,\varepsilon_m^-\right)$, the Hamiltonian of the Coulomb interaction is as follows:

$$\begin{aligned}H_{coul}\left(R_i,\varepsilon_m^-\right)=\frac{1}{2}\sum_{\vec{a}}\Big\{&W_{e-e}\left(\vec{R}_i;\vec{Q}\right)\left[\hat{\rho}_e\left(R_i;\vec{Q}\right)\hat{\rho}_e\left(R_i,-\vec{Q}\right)-\hat{N}_e\left(R_i\right)\right]\\&+W_{h-h}\left(\varepsilon_m^-;\vec{Q}\right)\left[\hat{\rho}_h\left(M_h,\varepsilon_m^-;\vec{Q}\right)\hat{\rho}_h\left(M_h,\varepsilon_m^-;\vec{Q}\right)-\hat{N}_h\left(M_h,\varepsilon_m^-\right)\right]\\&-2W_{e-h}\left(R_i,\varepsilon_m^-;\vec{Q}\right)\hat{\rho}_e\left(R_i;\vec{Q}\right)\hat{\rho}_h\left(M_h,\varepsilon_m^-;-\vec{Q}\right)\Big\}.\end{aligned}\tag{19}$$

Here, the electron and hole density operators are

$$\begin{gathered}\hat{\rho}_e\left(R_i;\vec{Q}\right)=\sum_t e^{iQ_y t l_0^2}a^+_{R_i,t+\frac{Q_x}{2}}a_{R_i,t-\frac{Q_x}{2}},\\ \hat{\rho}_h\left(M_h,\varepsilon_m^-;\vec{Q}\right)=\sum_t e^{-iQ_y t l_0^2}b^+_{M_h,\varepsilon_m^-,t+\frac{Q_x}{2}}b_{M_h,\varepsilon_m^-,t-\frac{Q_x}{2}},\\ \hat{N}_e\left(R_i\right)=\hat{\rho}_e\left(R_i,0\right);\ \hat{N}_h\left(M_h,\varepsilon_m^-\right)=\hat{\rho}_h\left(M_h,\varepsilon_m^-;0\right).\end{gathered}\tag{20}$$

Coefficients $W_{i-j}\left(Q\right)$ in the case of electron state R_1 described by formula (7) with coefficients a_0^- and b_1^- and the holes states $\left(M_h,\varepsilon_m^-\right)$ were deduced in [39]:

$$\begin{aligned}&W_{e-e}\left(R_1;\vec{Q}\right)=W\left(Q\right)\left(\left|a_0^-\right|^2A_{0,0}\left(\vec{Q}\right)+\left|b_1^-\right|^2A_{1,1}\left(\vec{Q}\right)\right)^2,\\&W_{h-h}\left(\varepsilon_m^-;\vec{Q}\right)=W\left(\vec{Q}\right)\left(\left|d_{m-3}^-\right|^2A_{m-3,m-3}\left(Q\right)+\left|c_m^-\right|^2A_{m,m}\left(Q\right)\right)^2,\ \mathrm{m}\geq 3\\&W_{e-h}\left(R_1,\varepsilon_m^-;\vec{Q}\right)=W\left(\vec{Q}\right)\left(\left|a_0^-\right|^2A_{0,0}\left(\vec{Q}\right)+\left|b_1^-\right|^2A_{1,1}\left(\vec{Q}\right)\right)\times\\&\times\left(\left|d_{m-3}^-\right|^2A_{m-3,m-3}\left(\vec{Q}\right)+\left|c_m^-\right|^2A_{m,m}\left(\vec{Q}\right)\right),\ m\geq 3.\end{aligned}\tag{21}$$

Coefficients $A_{i-i}\left(\vec{Q}\right)$ were obtained in [39].

Along with electron state R_1, we will consider state R_2 described by formulas (8). The combination of electron state R_2 with holes states ε_m^- gives rise to the e–h states$\left(eR_2,h,\varepsilon_m^-\right)$. Coefficients $W_{i-j}\left(R_2,\varepsilon_m^-;\vec{Q}\right)$ can be obtained from coefficients $W_{i-j}\left(R_1,\varepsilon_m^-;\vec{Q}\right)$ putting $b_1^-=0$ in them as follows

$$W_{i-j}\left(R_2,\varepsilon_m^-;\vec{Q}\right)=W_{i-j}\left(R_1,\varepsilon_m^-;\vec{Q}\right)\Big|_{b_1^-=0},\quad i,j=e,h.\tag{22}$$

The terms proportional to $\hat{N}_e(R_1)$ and $\hat{N}_h(M_h,\varepsilon_m^-)$ in (19) have coefficients $I_e(R_1)$ and $I_h(\varepsilon_m^-)$ describing the Coulomb self-actions of the electrons and holes. They are as follows:

$$I_e\left(R_1\right)=\frac{1}{2}\sum_{\vec{Q}}W_{e-e}\left(R_1,\vec{Q}\right);\ I_h\left(\varepsilon_m^-\right)=\frac{1}{2}\sum_{\vec{Q}}W_{h-h}\left(\varepsilon_m^-;\vec{Q}\right),$$
$$I_s\left(R_1,\varepsilon_m^-\right)=I_e\left(R_1\right)+I_h\left(\varepsilon_m^-\right). \tag{23}$$

To determine the binding energy of the magnetoexciton, wave functions $\left|\psi_{ex}\left(F_i,\vec{K}\right)\right\rangle$ were obtained by the author acting on vacuum state $\left|0\right\rangle$ by magnetoexciton creation operator $\psi_{ex}^{\dagger}(\vec{k}_{\|},M_h,R_i,\varepsilon)$ constructed from electron and hole creation operators $a_{R_i,t}^{\dagger}$ and $b_{M_h,\varepsilon,t}^{\dagger}$, respectively, as follows:

$$\psi_{ex}^{\dagger}\left(\vec{k}_{\|},R_i,M_h,\varepsilon\right)=\frac{1}{\sqrt{N}}\sum_t e^{ik_y t l_0^2}a^{\dagger}_{R_i,t+\frac{k_x}{2}}b^{\dagger}_{M_h,\varepsilon;\,-t+\frac{k_x}{2}},$$
$$\left|\psi_{ex}\left(R_i;M_h,\varepsilon;\vec{k}_{\|}\right)\right\rangle=\psi_{ex}^{\dagger}\left(\vec{k}_{\|},R_i,M_h,\varepsilon\right)\left|0\right\rangle. \tag{24}$$

The vacuum state is determined by the equalities

$$a_{\xi,t}\left|0\right\rangle=b_{\xi,t}\left|0\right\rangle=0. \tag{25}$$

Below, a particular composition $F_i=\left(R_1,M_h,\varepsilon_m^-\right)$ with $m\geq 3$ of the electron and hole states will be considered.

The binding energy of the magnetoexciton is determined by the diagonal matrix element of Hamiltonian (19) calculated with wave function $\left|\psi_{ex}\left(F_i,\vec{k}\right)\right\rangle$:

$$\left\langle\psi_{ex}\left(F_i,\vec{k}\right)\right|H_{coul}\left|\psi_{ex}\left(F_i,\vec{k}\right)\right\rangle=-I_{ex}\left(F_i\right)+E\left(F_i,\vec{k}\right),$$
$$I_{ex}\left(F_i\right)=I_{ex}\left(R_1,\varepsilon_m^-\right)=\sum_{\vec{Q}}W_{e-h}\left(R_1;\varepsilon_m^-;\vec{Q}\right),$$
$$E\left(F_i,\vec{k}\right)=E\left(R_1;\varepsilon_m^-;\vec{k}\right)=2\sum_{\vec{Q}}W_{e-h}\left(R_1;\varepsilon_m^-;\vec{Q}\right)\sin^2\left(\frac{\left[\vec{k}\times\vec{Q}\right]_z l_0^2}{2}\right), \tag{26}$$
$$\lim_{k\to\infty}E\left(R_1;\varepsilon_m^-;\vec{k}\right)=I_{ex}\left(R_1;\varepsilon_m^-\right).$$

The binding energy of the magnetoexciton and the magnetoexciton ionization potential, which has the opposite sign compared with that of the binding energy, tend to zero when wave vector $\vec{k}$ tends to infinity and the magnetoexciton is transformed into a free e–h pair.

The terms of the Hamiltonian, which contain only operators $\hat{N}_e$ and $\hat{N}_h$ describing the full numbers of electrons and holes including their chemical potentials μ_e and μ_h, are gathered in the form

$$H_{mex,1}=\left(\frac{E_g^0}{2}+E_e(R_1)-I_e(R_1)-\mu_e\right)\hat{N}_e(R_1)+$$
$$+\left(\frac{E_g^0}{2}+E_h(M_h,\varepsilon_m^-)-I_h(\varepsilon_m^-)-\mu_h\right)\hat{N}_h(M_h,\varepsilon_m^-). \tag{27}$$

Here, semiconductor energy band gap E_g^0 in the absence of LQ was introduced.

Now, instead of electron and hole density operators $\hat{\rho}_e(\vec{Q})$ and $\hat{\rho}_h(\vec{Q})$, we will introduce the density operators of the optical plasmon denoted as $\hat{\rho}(\vec{Q})$ and the acoustical plasmon denoted as $\hat{D}(\vec{Q})$ following the relations

$$\begin{gathered}\hat{\rho}(\vec{Q})=\hat{\rho}_e(\vec{Q})-\hat{\rho}_h(\vec{Q}),\ \hat{D}(\vec{Q})=\hat{\rho}_e(\vec{Q})+\hat{\rho}_h(\vec{Q}),\\ \hat{\rho}_e(\vec{Q})=\frac{\hat{\rho}(\vec{Q})+\hat{D}(\vec{Q})}{2},\ \hat{\rho}_h(\vec{Q})=\frac{\hat{D}(\vec{Q})-\hat{\rho}(\vec{Q})}{2}.\end{gathered} \tag{28}$$

Here, for simplicity, many indexes that label the electron, hole, and plasmon density operators are omitted. However, they must be kept in mind and may be restored in particular cases.

In the plasmon representation, Hamiltonian $H_{mex,1}$ (27) looks as follows:

$$H_{mex,1}=\left(E_{mex}(R_1;M_h,\varepsilon_m^-)-\mu_{mex}\right)\frac{\hat{D}(0)}{2}+\left(G_{e-h}(R_1;M_h,\varepsilon_m^-)-\mu_e+\mu_h\right)\frac{\hat{\rho}(0)}{2}. \tag{29}$$

Here, the sums and differences of the LQ level energies, the Coulomb self-interaction terms, and the chemical potentials are presented as follows:

$$\begin{gathered}E_{mex}(R_1;M_h,\varepsilon_m^-)=E_g(R_1;M_h,\varepsilon_m^-)-I_{ex}(R_1;\varepsilon_m^-),\\ E_g(R_1;M_h,\varepsilon_m^-)=E_g^0+E_e(R_1)+E_h(M_h,\varepsilon_m^-),\\ \mu_{ex}=\mu_e+\mu_h,\\ G_{e-h}(R_1;M_h,\varepsilon_m^-)=E_e(R_1)-E_h(M_h,\varepsilon_m^-)-I_e(R_1)+I_h(\varepsilon_m^-).\end{gathered} \tag{30}$$

The remaining part $H_{mex,2}$ of Hamiltonian (19) after the excluding of the linear terms is quadratic in the plasmon density operators. It has the form

$$\begin{gathered}H_{mex,2}=\frac{1}{2}\sum_{\vec{Q}}\Big\{W_{0-0}(\vec{Q})\hat{\rho}(\vec{Q})\hat{\rho}(-\vec{Q})+W_{a-a}(\vec{Q})\hat{D}(\vec{Q})\hat{D}(-\vec{Q})+\\ +W_{0-a}(\vec{Q})\left(\hat{\rho}(\vec{Q})\hat{D}(-\vec{Q})+\hat{D}(\vec{Q})\hat{\rho}(-\vec{Q})\right)\Big\}.\end{gathered} \tag{31}$$

The new coefficients are expressed in terms of the former ones by the formulas [40, 41]

$$\begin{gathered}W_{0-0}(\vec{Q})=\frac{1}{4}\left(W_{e-e}(\vec{Q})+W_{h-h}(\vec{Q})+2W_{e-h}(\vec{Q})\right),\\ W_{a-a}(\vec{Q})=\frac{1}{4}\left(W_{e-e}(\vec{Q})+W_{h-h}(\vec{Q})-2W_{e-h}(\vec{Q})\right),\\ W_{0-a}(\vec{Q})=\frac{1}{4}\left(W_{e-e}(\vec{Q})-W_{h-h}(\vec{Q})\right).\end{gathered} \tag{32}$$

The energy levels of LQ discussed above can be denoted as (e,R_i) for electrons and as (h,R_j) for the hhs. The LLLs for electrons are state $(e,R_1)=\left|\psi_0^-\right\rangle$ described by formulas (5)–(7) and state $(e,R_2)=\left|\psi_0\right\rangle$ determined by formula (8). For the hhs, the LLLs in the range of the magnetic field strength of $B\geq 10\,\mathrm{T}$ are states $\left|\psi_m^-\right\rangle$ with $m=3,4$ represented by formulas (13)–(15) and state $\left|\psi_0\right\rangle$ described by formula (17). It is evident from Figs. 3 and 4. This range of the magnetic field strength *B* is of special interest for the magnetoexciton physics, because it is this range in which the cyclotron energies for the electrons and holes are greater than the binding energy of the 2D Wannier–Mott excitons in GaAs-type crystals. Magnetoexcitons can exist only under these conditions. The range of weaker magnetic fields B is also of interest for the band-to-band optical quantum transitions. The renormalized energy band gap E_{cv} is greater than the E_g^0 value in the absence of an external magnetic field and equals to

$$E_{cv}(F_n) = E_g^0 + E_e(R_i) + E_h(R_j), \tag{33}$$

where F_n is the combination of states (e, R_i) and (h, R_j). We will consider six versions of F_n with $n = 1, 2, ..., 6$ appearing from the combinations of two electron states (e, R_i) with $i = 1, 2$ and three hole states (h, R_j) with $j = 1, 2, 3.$ They will be enumerated below. To create a magnetoexciton with wave vector $\vec{k} = 0,$ as a result of an optical quantum transition at point $\vec{k} = 0$ of the Brillouin zone, the photon energy should be smaller than renormalized band gap $E_{cv}(e, R_i; h, R_j)$ by the value of ionization potential $I_{ex}(e, R_i; h, R_j),$ calculated [33, 34] by the author as follows:

$$E_{mex}(e, R_i; h, R_j) = E_{cv}(e, R_i; h, R_j) - I_{ex}(e, R_i; h, R_j). \tag{34}$$

In the case of (e, R_i) and (h, ε_m^-), the respective ionization potentials are as follows:

$$I_{ex}(e, R_1; h, \varepsilon_m^-) = \sum_{\vec{Q}} W_{e-h}(R_1; \varepsilon_m^-; \vec{Q}) =$$

$$= |a_0^-|^2 |d_{m-3}^-|^2 I_{ex}^{(0,m-3)} + |a_0^-|^2 |c_m^-|^2 I_{ex}^{0,m} + |b_1^-|^2 |d_{m-3}^-|^2 I_{ex}^{(1,m-3)} + |b_1^-|^2 |c_m^-|^2 I_{ex}^{(1,m)}, \tag{35}$$

$$I_{ex}(e, R_2; h, \varepsilon_m^-) = \sum_{\vec{Q}} W_{e-h}(R_2; \varepsilon_m^-; \vec{Q}) = |d_{m-3}^-|^2 I_{ex}^{(0,m-3)} + |c_m^-|^2 I_{ex}^{(0,m)}.$$

Here, partial ionization potentials were introduced:

$$I_{ex}^{(p,q)} = \sum_{\vec{Q}} W_{e-h}(\vec{Q}) A_{p,p}(\vec{Q}) A_{q,q}(\vec{Q}). \tag{36}$$

The ionization potentials in the combinations $(e, R_i; h, \varepsilon_0)$ are

$$I_{ex}(e, R_1; h, \varepsilon_0) = |a_0^-|^2 I_{ex}^{(0,0)} + |b_1^-|^2 I_{ex}^{(1,0)}, \quad I_{ex}(e, R_2; h, \varepsilon_0) = I_{ex}^{(0,0)}. \tag{37}$$

The energies of the band-to-band optical quantum transitions accounted from semiconductor energy band gap E_g^0 in the absence of an external magnetic field, as well as the creation energies of magnetoexcitons at point $\vec{k} = 0$ in the same reference frame, are illustrated in Figs. 5–7 for six possible combinations of the electron and hole LLLs.

The $E_{cv}(F_n) - E_g^0$ dependences shown in Figs. 3 and 4 and the $E_{ex}(F_n, 0) - E_g^0$ dependences represented in Figs. 5–7 differ by the values of magnetoexciton ionization potentials $I_{ex}(F_n, 0)$ calculated at point $\vec{k} = 0$, where direct optical quantum transitions take place. For simplicity, they were denoted as $I_{ex}(F_n)$ [33–35]. Figure 5 shows the action of a strong perpendicular magnetic field giving rise to the LQ and the ZS of the 2D electrons and holes and to a change in the Coulomb e–h interaction. The additional action of a perpendicular electric field giving rise to the RSOC, as well as to the NP of the hh dispersion law, along with the LQ and the ZS induced by the magnetic field, is represented in Figs. 6 and 7.

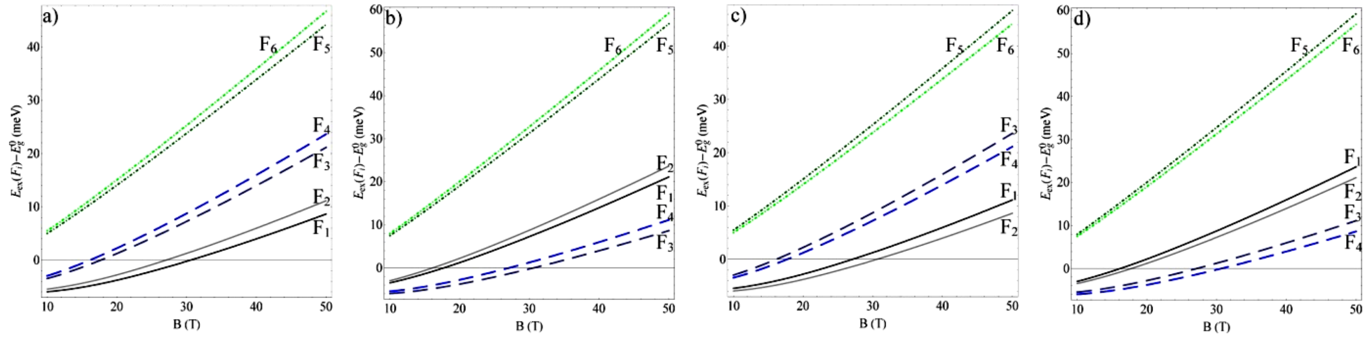

Fig. 5. *Reproduced, with permission, from* [40]: magnetoexciton energy levels $E_{ex}(F_i)-E_g^0$ for six combinations F_i of three hh and two electron LLLs as a function of magnetic field strength *B* at four combinations of the electron and hh *g*-factors g_e and g_h as follows: (a) $g_e=-1$, $g_h=-5$; (b) $g_e=-1$, $g_h=5$; (c) $g_e=1$, $g_h=-5$; and (d) $g_e=1$, $g_h=5$. The action of an external electric field is neglected taking the parameters $x=0$ and $C=0$.

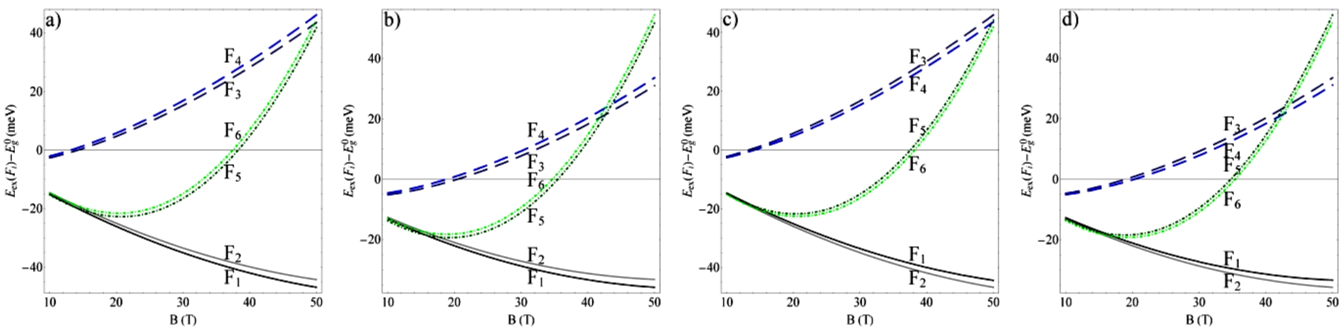

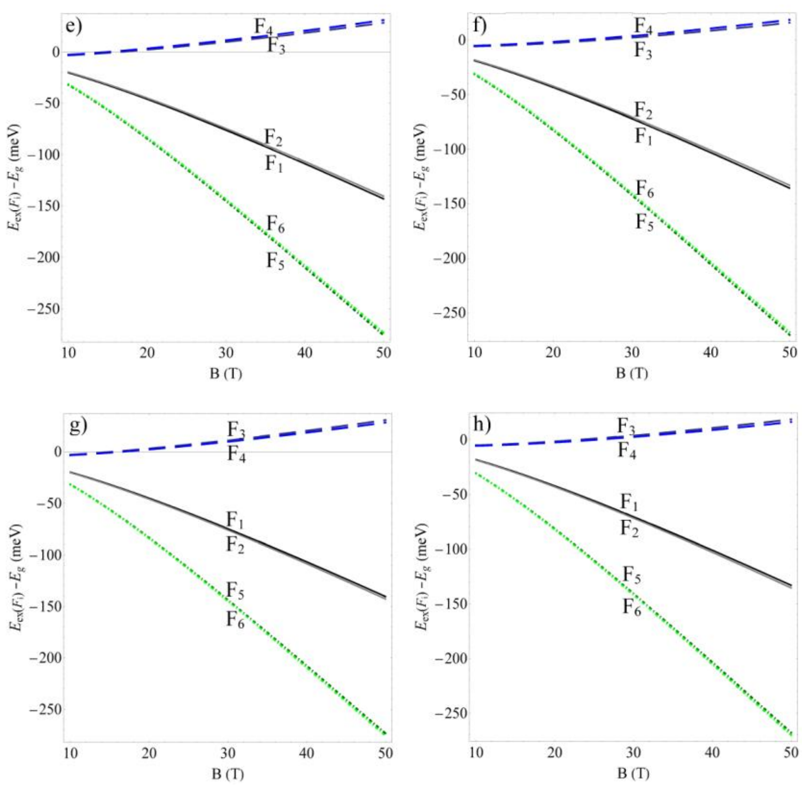

Fig. 6. Magnetoexciton energy levels $E_{ex}(F_i)-E_g^0$ for six combinations F_i of three hh and two electron LLLs as a function of magnetic field strength *B* at four combinations of the electron and hh *g*-factors g_e and g_h as follows: (a) $g_e=-1$, $g_h=-5$; (b) $g_e=-1$, $g_h=5$; (c) $g_e=1$, $g_h=-5$; and (d) $g_e=1$, $g_h=5$. The action of an external electric field is taken into account using the parameters $x=30$ and $C=30$. Figures 6a–6d are reproduced, with permission, from [40]. The case of parameters $x=30$ and $C=10$ is considered in the set of Figs. 6e–6h with electron and hh *g*-factors applicable to their variation in Figs. 6a–6d, respectively.

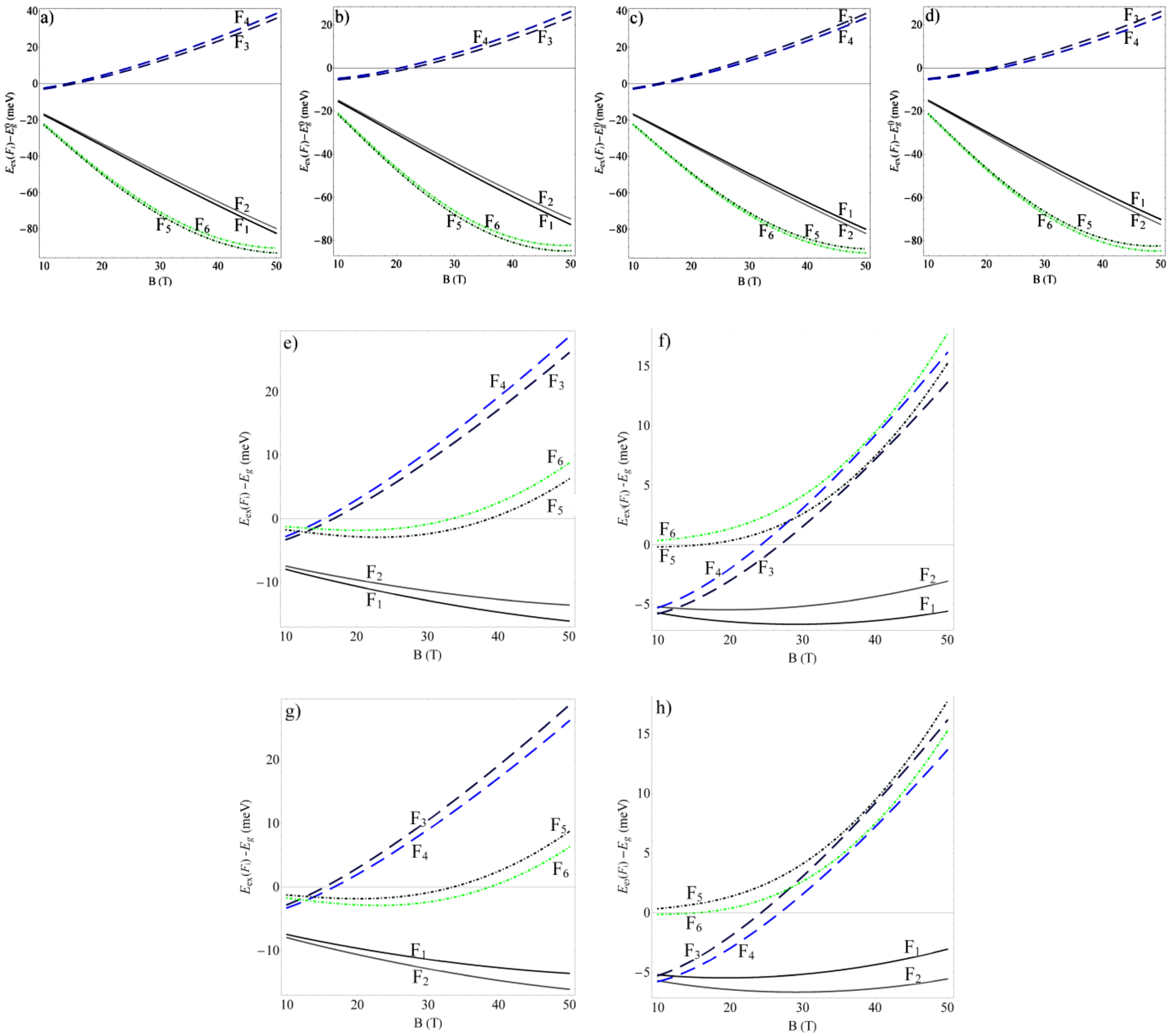

Fig. 7. Magnetoexciton energy levels $E_{ex}(F_i)-E_g^0$ for six combinations F_i of three hh and two electron LLLs as a function of magnetic field strength B at four combinations of the electron and hh g-factors g_e and g_h as follows: (a, e) $g_e=-1$, $g_h=-5$; (b, f) $g_e=-1$, $g_h=5$; (c, g) $g_e=1$, $g_h=-5$; and (d, h) $g_e=1$, $g_h=5$. The action of an external electric field is taken into account using the parameters x = 30 and C = 20 for Figs. 7a–7d [40] and x = 10 and C = 20 for Figs. 7e–7h.

They are characterized by parameters x and C. Recall that the introduction of the NP of the dispersion law is required to compensate the action of the third-order chirality terms in Hamiltonian (10); otherwise, the usual picture of the semiconductor energy band gap will be destroyed due to the unlimited penetration of the hh energy levels inside the band gap.

Comparison of Figs. 6 and 7 shows that a decrease in the NP parameter C leads to significant penetration of the energy levels into the range of negative values.

In a more general case of $\vec{k} \neq 0$, these combinations are as follows:

$$E_{ex}(F_n, \vec{k}_{\|}) = E_{cv}(F_n) - I_{ex}(F_n, \vec{k}_{\|}),$$
$$I_{ex}(F_n; 0) = I_{ex}(F_n), \tag{38}$$
$$E_{cv}(F_n) - E_g^0 = E_e(R_i) + E_h(R_j), \;\; n = 1, \ldots 6, \;\; i = 1, 2, \;\; j = 1, 2, 3.$$

In the next section, the ionization potentials of magnetoexcitons at arbitrary values of wave vectors $\vec{k}_{\|}$ will be required to describe the polariton dispersion law. Particular expressions [33–35] were obtained by the author:

$$\begin{aligned}
&F_1 = (e, R_1; h, \varepsilon_3^-), \;\; E_{cv}(F_1) - E_g^0 = E_e(R_1) + E_h(\varepsilon_3^-),\\
&I_{ex}(F_1; \vec{k}_{\|}) = I_{ex}(e, R_1; h, \varepsilon_3^-; \vec{k}_{\|}) =\\
&= \left|a_0^-\right|^2 \left|d_0^-\right|^2 I_{ex}^{(0,0)}\left(\vec{k}_{\|}\right) + \left|a_0^-\right|^2 \left|c_3^-\right|^2 I_{ex}^{(0,3)}\left(\vec{k}_{\|}\right) + \left|b_1^-\right|^2 \left|d_0^-\right|^2 I_{ex}^{(1,0)}\left(\vec{k}_{\|}\right) + \left|b_1^-\right|^2 \left|c_3^-\right|^2 I_{ex}^{(1,3)}\left(\vec{k}_{\|}\right),\\
&F_2 = (e, R_2; h, \varepsilon_3^-), \;\; E_{cv}(F_2) - E_g^0 = E_e(R_2) + E_h(\varepsilon_3^-),\\
&I_{ex}(F_2; \vec{k}_{\|}) = I_{ex}(e, R_2; h, \varepsilon_3^-; \vec{k}_{\|}) = \left|d_0^-\right|^2 I_{ex}^{(0,0)}\left(\vec{k}_{\|}\right) + \left|c_3^-\right|^2 I_{ex}^{(0,3)}\left(\vec{k}_{\|}\right),\\
&F_3 = (e, R_1; h, \varepsilon_0), \;\; E_{cv}(F_3) - E_g^0 = E_e(R_1) + E_h(\varepsilon_0),\\
&I_{ex}(F_3; \vec{k}_{\|}) = I_{ex}(e, R_1; h, \varepsilon_0; \vec{k}_{\|}) = \left|a_0^-\right|^2 I_{ex}^{(0,0)}\left(\vec{k}_{\|}\right) + \left|b_1^-\right|^2 I_{ex}^{(1,0)}\left(\vec{k}_{\|}\right),\\
&F_4 = (e, R_2; h, \varepsilon_0), \;\; E_{cv}(F_4) - E_g^0 = E_e(R_2) + E_h(\varepsilon_0),\\
&I_{ex}(F_4; \vec{k}_{\|}) = I_{ex}(e, R_2; h, \varepsilon_0; \vec{k}_{\|}) = I_{ex}^{(0,0)}\left(\vec{k}_{\|}\right),\\
&F_5 = (e, R_1; h, \varepsilon_4^-), \;\; E_{cv}(F_5) - E_g^0 = E_e(R_1) + E_h(\varepsilon_4^-),\\
&I_{ex}(F_5; \vec{k}_{\|}) = I_{ex}(e, R_1; h, \varepsilon_4^-; \vec{k}_{\|}) =\\
&= \left|a_0^-\right|^2 \left|d_1^-\right|^2 I_{ex}^{(0,1)}\left(\vec{k}_{\|}\right) + \left|a_0^-\right|^2 \left|c_4^-\right|^2 I_{ex}^{(0,4)}\left(\vec{k}_{\|}\right) + \left|b_1^-\right|^2 \left|d_1^-\right|^2 I_{ex}^{(1,1)}\left(\vec{k}_{\|}\right) + \left|b_1^-\right|^2 \left|c_4^-\right|^2 I_{ex}^{(1,4)}\left(\vec{k}_{\|}\right),\\
&F_6 = (e, R_2; h, \varepsilon_4^-), \;\; E_{cv}(F_6) - E_g^0 = E_e(R_2) + E_h(\varepsilon_4^-),\\
&I_{ex}(F_6; \vec{k}_{\|}) = I_{ex}(e, R_2; h, \varepsilon_4^-; \vec{k}_{\|}) = \left|d_1^-\right|^2 I_{ex}^{(0,1)}\left(\vec{k}_{\|}\right) + \left|c_4^-\right|^2 I_{ex}^{(0,4)}\left(\vec{k}_{\|}\right).
\end{aligned} \tag{39}$$

They consist of partial ionization potentials $I_{ex}^{(n,m)}\left(\vec{k}_{\|}\right)$. Some of them are listed below together with their series expansions in terms of small variable $\vec{k}_{\|}^2 l_0^2 < 1$:

$$I_{ex}^{(0,0)}\left(\vec{k}_{\|}\right) = I_l e^{-\frac{\vec{k}_{\|}^2 l_0^2}{2}} {}_1F_1\left(\frac{1}{2}, 1, \frac{\vec{k}_{\|}^2 l_0^2}{2}\right) \approx I_l\left(1 - \frac{\vec{k}_{\|}^2 l_0^2}{4}\right),$$

$$I_{ex}^{(1,0)}\left(\vec{k}_{\|}\right) = I_l e^{-\frac{\vec{k}_{\|}^2 l_0^2}{2}} \left[{}_1F_1\left(\tfrac{1}{2}, 1, \frac{\vec{k}_{\|}^2 l_0^2}{2}\right) - \tfrac{1}{2}\, {}_1F_1\left(-\tfrac{1}{2}, 1, \frac{\vec{k}_{\|}^2 l_0^2}{2}\right)\right] \approx I_l\left(\frac{1}{2} + \frac{1}{8}\vec{k}_{\|}^2 l_0^2\right),$$

$$I_{ex}^{(0,3)}\left(\vec{k}_{\|}\right)=I_l e^{-\frac{\vec{k}_{\|}^2 l_0^2}{2}}\left[{}_1F_1\left(\frac{1}{2},1,\frac{\vec{k}_{\|}^2 l_0^2}{2}\right)-\frac{3}{2}{}_1F_1\left(-\frac{1}{2},1,\frac{\vec{k}_{\|}^2 l_0^2}{2}\right)+\right.$$
$$\left.+\frac{9}{8}{}_1F_1\left(-\frac{3}{2},1,\frac{\vec{k}_{\|}^2 l_0^2}{2}\right)-\frac{5}{16}{}_1F_1\left(-\frac{5}{2},1,\frac{\vec{k}_{\|}^2 l_0^2}{2}\right)\right]\approx I_l\left(\frac{5}{16}+\frac{1}{64}\vec{k}_{\|}^2 l_0^2\right),$$
$$I_{ex}^{(1,3)}\left(\vec{k}_{\|}\right)=I_l e^{-\frac{\vec{k}_{\|}^2 l_0^2}{2}}\left[{}_1F_1\left(\frac{1}{2},1,\frac{\vec{k}_{\|} l_0^2}{2}\right)-2\,{}_1F_1\left(-\frac{1}{2},1,\frac{\vec{k}_{\|} l_0^2}{2}\right)+\frac{27}{8}\times\right.$$
$$\left.\times{}_1F_1\left(-\frac{3}{2},1,\frac{\vec{k}_{\|}^2 l_0^2}{2}\right)-\frac{25}{8}{}_1F_1\left(-\frac{5}{2},1,\frac{\vec{k}_{\|}^2 l_0^2}{2}\right)+\frac{35}{32}{}_1F_1\left(-\frac{7}{2},1,\frac{\vec{k}_{\|}^2 l_0^2}{2}\right)\right]\approx I_l\left(\frac{11}{32}+\frac{5}{128}\vec{k}_{\|}^2 l_0^2\right). \quad (40)$$

These series expansions including the terms proportional to $\vec{k}_{\|}^2 l_0^2$ give the possibility to determine magnetic mass $M(F_1,B)$ of the magnetoexciton in state F_1 as follows:

$$I_{ex}\left(F_1,B,\vec{k}_{\|}\right)=I_l A\left(F_1,B\right)-I_l\frac{\vec{k}_{\|}^2 l_0^2}{2}G\left(F_1,B\right)=I_{ex}\left(F_1,B,0\right)-\frac{\hbar^2\vec{k}_{\|}^2}{2M(F_1,B)}. \quad (41)$$

Here, denotations $A\left(F_1,B\right)$ and $G\left(F_1,B\right)$ were introduced:

$$I_{ex}\left(F_1,B,0\right)=I_l A\left(F_1,B\right),\quad M\left(F_1,B\right)=\frac{\hbar^2}{I_l l_0^2 G\left(F_1,B\right)},$$
$$A\left(F_1,B\right)=\left|d_0^-\right|^2\cdot\left(\left|a_0^-\right|^2+\frac{1}{2}\left|b_1^-\right|^2\right)+\frac{1}{16}\left|c_3^-\right|\left(5\left|a_0^-\right|^2+\frac{11}{2}\left|b_1^-\right|^2\right), \quad (42)$$
$$G\left(F_1,B\right)=\frac{1}{2}\left|a_0^-\right|^2\left(\left|d_0^-\right|^2-\frac{1}{16}\left|c_3^-\right|^2\right)-\frac{1}{4}\left|b_1^-\right|^2\left(\left|d_0^-\right|^2+\frac{5}{16}\left|c_3^-\right|^2\right).$$

In the case of dipole-active state F_4 the ionization potential is $I_{ex}^{(0,0)}\left(\vec{k}_{\|}\right)$ and has magnetic mass $M\left(F_4,B\right)$ determined in [9]. The both masses are shown below:

$$M\left(F_4,B\right)=\frac{2\hbar^2}{I_l l_0^2},\quad M\left(F_1,B\right)=\frac{\sqrt{2}\hbar^2\varepsilon_0}{\sqrt{\pi}e^2 l_0 G\left(F_1,B\right)},\quad I_l=\frac{e^2}{\varepsilon_0 l_0}\sqrt{\frac{\pi}{2}}. \quad (43)$$

They depend on the magnetic field strength. Their expressions in dimensionless form related to free electron mass m_0, namely, $M\left(F_4,B\right)/m_0$ and $M\left(F_1,B\right)/m_0$, are represented in Fig. 8.

The accumulated knowledge about 2D magnetoexcitons will be supplemented below by their interaction with photons confined in a microcavity giving rise to the formation of polaritons.

4. Interaction of Magnetoexcitons with Electromagnetic Radiation and the Formation of Cavity Polaritons [40]

The authors of [27, 33, 36, 39] deduced Hamiltonians describing, in different approximations, the electron–radiation interaction in a system of two-dimensional coplanar electrons and holes accumulated in a semiconductor QW and subjected to the action of a strong perpendicular magnetic field giving rise to the LQ of their energy levels. Only the case of the inter-band optical quantum transitions with the creation or annihilation of one e–h pair in [27, 33, 36, 39] was considered. The intra-band quantum transitions were discussed in [31]. The authors of [33] studied the exciton–cyclotron resonance and the optical orientation phenomena [42] arising under the action of circularly polarized laser radiation without taking into account the RSOC. The Hamiltonian deduced in [33] in the e–h representation was transcribed in [27] so as to describe the magnetoexciton–photon interaction for the light propagating arbitrarily in the three-dimensional (3D) space as well as being confined in a microcavity. The dispersion law of the magnetoexciton–polariton in a microcavity was deduced. The dependence of the Rabi frequency on the magnetic field strength, as well as the selection rule concerning the numbers of the LQ levels of the e–h pair engaged in the dipole-active and quadrupole-active transitions, were determined [27]. The effect on the optical properties of the magnetoexcitons and the band-to-band quantum transitions of the RSOC arising due to the action of a supplementary electric field perpendicular to the plane of the QW was investigated in [34–36, 39]. The third-order chirality terms in Hamiltonian (1) of the hh induced by the electric field obliged one to introduce an additional NP term of the same origin in the hh dispersion law. The NP term, together with the chirality terms, essentially change the dependence of the energy levels on the magnetic field strength, as evidenced by Figs. 2, 4, 6, and 7. The role of the NP term is to prevent the unlimited deep penetration of the energy levels of the 2D hh, as well as the e–h pair and the magnetoexciton, inside the energy band gap and contribute to the stability of the semiconductor band structure. The authors of [34–36, 39] did not discuss the effects related with the ZS. This lack is removed below. We will discuss the properties of magnetoexcitons and magnetoexciton–polaritons [40] taking into account the effect of a full set of four factors, such as LQ, RSOC, ZS, and NP. The Hamiltonian describing the magnetoexciton–photon interaction including the ZS effects looks exactly the same as in [36] with only one difference that coefficients a_0^-, b_1^-, c_m^-, and d_{m-3}^- with $m \geq 3$ should be determined by expressions (5) and (14) containing nonzero Zeeman coefficients Z_e and Z_h. These coefficients were absent in previous papers [34–36, 39].

Following formula (41) of [36], the Hamiltonian of the magnetoexciton–photon interaction looks as follows:

$$\begin{aligned}
&\hat{H}_{e-rad} = \left(-\frac{e}{m_0 l_0}\right) \sum_{\vec{k}(\vec{k}_\parallel, k_z)} \sum_{M_h=\pm 1} \sum_{i=1,2} \sum_{\varepsilon=\varepsilon_m, \varepsilon_m^-} \sqrt{\frac{\hbar}{L_z \omega_{\vec{k}}}} \times \\
&\times \Big\{ P_{cv}(0) T\left(R_i, \varepsilon, \vec{k}_\parallel\right) \Big[C_{\vec{k},-}\left(\vec{\sigma}_{\vec{k}}^{+} \cdot \vec{\sigma}_{M_h}^{*}\right) + C_{\vec{k},+}\left(\vec{\sigma}_{\vec{k}}^{-} \cdot \vec{\sigma}_{M_h}^{*}\right) \Big] \hat{\Psi}_{ex}^{\dagger}(\vec{k}_\parallel, M_h, R_i, \varepsilon) + \\
&+ P^{*}_{cv}(0) T^{*}\left(R_i, \varepsilon, \vec{k}_\parallel\right) \Big[\left(C_{\vec{k},-}\right)^{\dagger} \left(\vec{\sigma}_{\vec{k}}^{-} \cdot \vec{\sigma}_{M_h}\right) + \left(C_{\vec{k},+}\right)^{\dagger} \left(\vec{\sigma}_{\vec{k}}^{+} \cdot \vec{\sigma}_{M_h}\right) \Big] \hat{\Psi}_{ex}(\vec{k}_\parallel, M_h, R_i, \varepsilon) + \\
&+ P_{cv}(0) T\left(R_i, \varepsilon, -\vec{k}_\parallel\right) \Big[\left(C_{\vec{k},-}\right)^{\dagger} \left(\vec{\sigma}_{\vec{k}}^{-} \cdot \vec{\sigma}_{M_h}^{*}\right) + \left(C_{\vec{k},+}\right)^{\dagger} \left(\vec{\sigma}_{\vec{k}}^{+} \cdot \vec{\sigma}_{M_h}^{*}\right) \Big] \hat{\Psi}_{ex}^{\dagger}(-\vec{k}_\parallel, M_h, R_i, \varepsilon) + \\
&+ P^{*}_{cv}(0) T^{*}\left(R_i, \varepsilon, -\vec{k}_\parallel\right) \Big[C_{\vec{k},-}\left(\vec{\sigma}_{\vec{k}}^{+} \cdot \vec{\sigma}_{M_h}\right) + C_{\vec{k},+}\left(\vec{\sigma}_{\vec{k}}^{-} \cdot \vec{\sigma}_{M_h}\right) \Big] \hat{\Psi}_{ex}(-\vec{k}_\parallel, M_h, R_i, \varepsilon) \Big\}.
\end{aligned} \tag{44}$$

It differs from Hamiltonian (9) in [27] by more complicate coefficients $T\left(R_i, \varepsilon, \vec{k}_\parallel\right)$, which in turn now contain generalized coefficients a_0^-, b_1^-, c_m^-, and d_{m-3}^- given by expressions (5) and (14). Hamiltonian (44) contains the creation and annihilation operators of the magnetoexcitons $\hat{\Psi}_{ex}^{\dagger}(\vec{k}_\parallel, M_h, R_i, \varepsilon)$, $\hat{\Psi}_{ex}(\vec{k}_\parallel, M_h, R_i, \varepsilon)$ and the photons $C_{\vec{k},\xi}^{\dagger}$, $C_{\vec{k},\xi}$. First of them were determined by formula (24) and are characterized by in-plane wave vectors $\vec{k}_\parallel$ by orbital projection M_h of the hole state in the frame of the *p*-type valence band and by quantum states R_i and ε of the electron and hole under conditions of the LQ accompanied by the RSOC, ZS, and NP. Instead of quantum number M_h, circular polarization vector $\vec{\sigma}_{M_h}$ will be introduced. The photon operators depend on wave vectors $\vec{k}=\vec{a}_3 k_z+\vec{k}_{\parallel}$ arbitrarily oriented in the 3D space, where $\vec{a}_3$ is an unit vector perpendicular to the layer, and on polarization label ξ, which takes two values 1 and 2 in the case of the light with linear polarizations $\vec{e}_{\vec{k},i}$ or signs $\pm$ in the case of circular polarizations $\vec{\sigma}_{\vec{k}}^{\pm}$. The required denotations are

$$
\begin{gathered}
C_{\vec{k},\pm}=\frac{1}{\sqrt{2}}\left(C_{\vec{k},1}\pm iC_{\vec{k},2}\right),\ \left(C_{\vec{k},\pm}\right)^{\dagger}=\frac{1}{\sqrt{2}}\left(C_{\vec{k},1}^{\dagger}\mp iC_{\vec{k},2}^{\dagger}\right),\\
\vec{\sigma}_{\vec{k}}^{\pm}=\frac{1}{\sqrt{2}}\left(\vec{e}_{\vec{k},1}\pm i\vec{e}_{\vec{k},2}\right),\ \left(\vec{e}_{\vec{k},1}\cdot\vec{k}\right)=0,\ i=1,2,\\
\sum_{i=1}^{2}C_{\vec{k},i}\vec{e}_{\vec{k},i}=C_{\vec{k},-}\vec{\sigma}_{\vec{k}}^{+}+C_{\vec{k},+}\vec{\sigma}_{\vec{k}}^{-},\quad \sum_{i=1}^{2}\left(C_{\vec{k},\pm}\right)^{\dagger}\vec{e}_{\vec{k},i}=\left(C_{\vec{k},-}\right)^{\dagger}\vec{\sigma}_{\vec{k}}^{-}+\left(C_{\vec{k},+}\right)^{\dagger}\vec{\sigma}_{\vec{k}}^{+},\\
\vec{\sigma}_{M_h}=\frac{1}{\sqrt{2}}(\vec{a}_1\pm i\vec{a}_2),\ \vec{k}_{\parallel}=k_x\vec{a}_1+k_y\vec{a}_2,\ \left(\vec{\sigma}_{M_h}\cdot\vec{a}_3\right)=0,\ M_h=\pm 1.
\end{gathered}
\tag{45}
$$

Here, $\vec{a}_1$ and $\vec{a}_2$ are the in-plane orthogonal unit vectors. Scalar products $\left(\vec{\sigma}_{\vec{k}}^{\pm}\cdot\vec{\sigma}_{M_h}^{*}\right)$ appearing in Hamiltonian (44) determine the ability of photon circular polarization $\vec{\sigma}_{\vec{k}}^{\pm}$ to create a circular polarization $\vec{\sigma}_{M_h}$ with probability $\left|\left(\vec{\sigma}_{\vec{k}}^{\pm}\cdot\vec{\sigma}_{M_h}^{*}\right)\right|^2$. It can be denoted as a geometrical selection rule. This probability is the same for any in-plane wave vector $\vec{k}=\vec{k}_{\parallel}$ and equals to 1/4. In the case of incident wave vector $\vec{k}$ perpendicular to the layer $\vec{k}=\vec{a}_3 k_z$ the light with circular polarization $\vec{\sigma}_{\vec{k}}^{\pm}$ excites the magnetoexciton with the same circular polarization $\vec{\sigma}_{M_h}=\vec{\sigma}_{\vec{k}}^{\pm}$ with the probability equal to unity. Other spin–orbital selection rules are determined by coefficients $T\left(R_i,\varepsilon,\vec{k}_{\parallel}\right)$, which are expressed by formulas (36) in [36] as follows:

$$
\begin{gathered}
T\left(R_1,\varepsilon_m^{-};\vec{k}_{\parallel}\right)=a_0^{-*}d_{m-3}^{-*}\tilde{\phi}\left(0,m-3;\vec{k}_{\parallel}\right)-b_1^{-*}c_m^{-*}\tilde{\phi}\left(1,m;\vec{k}_{\parallel}\right),\ m\geq 3,\\
T\left(R_1,\varepsilon_m;\vec{k}_{\parallel}\right)=-b_1^{-*}\tilde{\phi}\left(1,m;\vec{k}_{\parallel}\right),\ m=0,1,2,\\
T\left(R_2,\varepsilon_m^{-};\vec{k}_{\parallel}\right)=-c_m^{-*}\tilde{\phi}\left(0,m;\vec{k}_{\parallel}\right),\ m\geq 3,\\
T\left(R_2,\varepsilon_m;\vec{k}_{\parallel}\right)=-\tilde{\phi}\left(0,m;\vec{k}_{\parallel}\right),\ m=0,1,2.
\end{gathered}
\tag{46}
$$

Integrals $\tilde{\phi}\left(n_e,n_h;\vec{k}_{\parallel}\right)$ were introduces by formulas (32) of [36]. They have a general form and some particular values given below

$$
\begin{gathered}
\tilde{\phi}\left(n_e,n_h;\vec{k}_{\parallel}\right)=\int_{-\infty}^{\infty}dy\varphi_{n_e}\left(y-\frac{k_x l_0^2}{2}\right)\varphi_{n_h}\left(y+\frac{k_x l_0^2}{2}\right)e^{ik_y y},\\
\tilde{\phi}\left(0,0;\vec{k}_{\parallel}\right)=1-\left(\frac{k_x^2}{2}+k_y^2\right)\frac{l_0^2}{4},\quad \tilde{\phi}\left(0,1;\vec{k}_{\parallel}\right)=\frac{\left(k_x+ik_y\right)l_0}{\sqrt{2}}.
\end{gathered}
\tag{47}
$$

At point $\vec{k}_{\parallel}=0$ they coincide with the normalization and the orthogonality conditions for wave functions $\varphi_n(y)$, which have real values.

Integrals (47) play the role of orbital selection rules for the quantum transitions from the ground state of the crystal to the magnetoexciton states and for the band-to-band optical transitions. Following them in the case of the dipole-active transitions with $\vec{k}_{\parallel}=0$, the selection rule is $n_e=n_h$. In the case of quadrupole-active quantum transitions, their amplitudes are proportional to $\left(k_x+ik_y\right)l_0$ and their probabilities are proportional to $\vec{k}_{\parallel}^2 l_0^2$, which is a small factor on the order of $\left(l_0/\lambda\right)^2<<1$, where λ is the light wavelength. In this case, following (47), the difference between quantum numbers n_e and n_h satisfies the following requirements: $n_e=n_h\pm 1$. Selection rules (47) allow also higher order multi-pole quantum transitions with probabilities on the order of $\left(l_0/\lambda\right)^{2n}$ with $n>1$; however, these infinitesimal values will be neglected and the respective quantum transitions will be considered for simplicity forbidden. We will discuss two types of the allowed inter-band quantum transitions. During the dipole-active transitions with $\vec{k}_{\parallel}=0$, quantum numbers n_e and n_h of the electron and hh LQ states coincide, i.e., $n_e=n_h$.

During the quadrupole-active quantum transitions, the probabilities are proportional to a small factor $\left(\vec{k}_{\parallel}l_0\right)^2$, whereas quantum numbers n_e and n_h satisfy requirements $n_e=n_h\pm 1$, as follows from expressions (47). The quantum transitions in magnetoexciton state F_1 composed of electron state R_1 and state ε_3^-, which means $F_1=\left(R_1,\varepsilon_3^-\right)$, is determined by coefficient $T\left(R_1,\varepsilon_3^-,\vec{k}_{\parallel}\right)$ written in list (46). It has a specific expression

$$T(F_1,\vec{k}_{\parallel})=T\left(R_1,\varepsilon_3^-,\vec{k}_{\parallel}\right)=a_0^{-*}d_0^{-*}\tilde{\phi}\left(0,0;\vec{k}_{\parallel}\right)-b_1^{-*}c_3^{-*}\tilde{\phi}\left(1,3;\vec{k}_{\parallel}\right)\approx a_0^{-*}d_0^{-*}. \tag{48}$$

Magnetoexciton state F_1 is dipole-active with the probability of the quantum transition proportional to $|a_0^-|^2|d_0^-|^2$. State F_1 described above in the presence of the RSOC, ZS, and NP term is a successor of a state with $M_h=-1$ discussed in [27, 33] in the absence of RSOC. To verify this statement, one can analyze the energy spectra for electron state ε_0^- (5) and for hh state ε_3^- (13) directing their chirality term parameters α and β including the NP term δ to zero. In this case, we will obtain the following expressions: $\underset{\alpha\to 0}{\varepsilon_0^-}=1/2+Z_e$ and $\underset{\beta\to 0,\delta\to 0}{\varepsilon_3^-}=1/2+Z_h$. In this limit, we can see that the electron spin projection is $S_z^e=1/2$, whereas the hh effective spin projection $\tilde{S}_z^h$ equals –1/2, which is equivalent to the full angular momentum projection $j_z^h=-3/2$. However, a hh spinor-type wave function with quantum number $j_z^h=-3/2$ can be constructed only with the orbital periodic part of the *p*-type valence band wave function with quantum number $M_h=-1$. As a result, state $F_1=(R_1,\varepsilon_3^-)$ in the limit of the small chirality terms is characterized by summary angular projection $j_z^{e-h}=S_z^e+j_z^h$ equal to –1 and, at the same time, by quantum number $M_h = -1$. In fact, state $F_1 = (R_1, \varepsilon_3^-)$ is a successor of the state with $M_h = -1$ discussed in [9, 21] in the absence of RSOC. This state is dipole-active. Another dipole-active state has the following composition: $F_4 = (R_2, \varepsilon_0)$. In the case of vanishing chirality term parameters α, β, and δ, the energy spectra are $\underset{\alpha\to 0}{\varepsilon_0^{(e)}} = 1/2 - Z_e$ and $\underset{\beta\to 0,\delta\to 0}{\varepsilon_0^{(h)}} = 1/2 - Z_h$. They are characterized by electron spin projection $S_z^e = -1/2$ and hh quantum numbers $\tilde{S}_z^h = 1/2$, $j_z^h = 3/2$, and $M_h = 1$. This state in the limit of small chirality terms is characterized by quantum numbers $j_z^{e-h} = S_z^e + j_z^h = 1$ and $M_h = 1$. It is a successor of the state with $M_h = 1$ discussed in [27, 33] in the absence of RSOC. Coefficient $T\left(R_2, \varepsilon_0; \vec{k}_{\parallel}\right)$ looks as follows:

$$T(F_4, \vec{k}_{\parallel}) = T\left(R_2, \varepsilon_0; \vec{k}_{\parallel}\right) = -\tilde{\phi}\left(0, 0; \vec{k}_{\parallel}\right) \approx -1. \tag{49}$$

Two of the six initially selected lowest magnetoexciton states are quadrupole-active. They have e–h combinations $F_3 = \left(R_1, \varepsilon_0\right)$ and $F_5 = \left(R_1, \varepsilon_4^-\right)$. In both cases, the electron energy spectrum in the limit $\alpha \to 0$ looks as $\underset{\alpha\to 0}{\varepsilon_0} = 1/2 + Z_e$ and has quantum number $S_z^e = 1/2$. The two hh states ε_0 and ε_4^- in the limit $\beta \to 0$, $\delta \to 0$ have the form $\underset{\beta\to 0,\delta\to 0}{\varepsilon_0} = 1/2 - Z_h$ and $\underset{\beta\to 0,\delta\to 0}{\varepsilon_4^-} = 3/2 + Z_h$. State $F_3 = \left(R_1, \varepsilon_0\right)$ is characterized by quantum numbers $S_z^e = -1/2$, $\tilde{S}_z^h = 1/2$, $j_z^h = 3/2$, $M_h = 1$, and $J_z^{e-h} = 2$. Coefficient $T\left(R_1, \varepsilon_0; \vec{k}_{\parallel}\right)$ equals to

$$T(F_3, \vec{k}_{\parallel}) = T\left(R_1, \varepsilon_0; \vec{k}_{\parallel}\right) = -b_1^{-*}\tilde{\phi}\left(1, 0; \vec{k}_{\parallel}\right) = -b_1^{-*}\left(\frac{-k_x + ik_y}{\sqrt{2}}\right) l_0. \tag{50}$$

It is a small quadrupole-active transition due to a difference between the values of $J_z^{e-h} = 2$ and $M_h = 1$ and a small value of coefficient b_1^- in the case of small chirality terms. State $F_5 = \left(R_1, \varepsilon_4^-\right)$, unlike state $F_3 = \left(R_1, \varepsilon_0\right)$, has quantum numbers $S_z^e = 1/2$, $\tilde{S}_z^h = -1/2$, $j_z^h = -3/2$, $M_h = -1$, and $J_z^{e-h} = -1$. Coefficient $T\left(R_1, \varepsilon_4^-; \vec{k}_{\parallel}\right)$ looks as follows:

$$T(F_5, \vec{k}_{\parallel}) = T\left(R_1, \varepsilon_4^-; \vec{k}_{\parallel}\right) = a_0^{-*}d_0^{-*}\tilde{\phi}\left(0, 1; \vec{k}_{\parallel}\right) - b_1^{-*}c_4^{-*}\tilde{\phi}\left(1, 4; \vec{k}_{\parallel}\right) \approx a_0^{-*}d_0^{-*}\left(\frac{k_x + ik_y}{\sqrt{2}}\right) l_0. \tag{51}$$

In the same case of a small chirality terms, coefficients a_0^- and d_0^- can approach unity and this quadrupole transition is more significant than the previous one.

The last two states $F_2 = \left(R_2, \varepsilon_3^-\right)$ and $F_6 = \left(R_2, \varepsilon_4^-\right)$ are forbidden. Both of them have electron state $\underset{\alpha\to 0}{\varepsilon_0} = 1/2 - Z_e$ and hole states $\underset{\beta\to 0,\delta\to 0}{\varepsilon_m^-} = (m-1) - 3/2 + Z_h$ with $m = 3, 4$. They are characterized by quantum numbers $S_z^e = -1/2$, $\tilde{S}_z^h = -1/2$, $j_z^h = -3/2$, $M_h = -1$, and $J_z^{e-h} = -2$ Their coefficients $T\left(R_2, \varepsilon_m^-; \vec{k}_{\parallel}\right)$ with $m = 3, 4$ are as follows:

$$T\left(R_2, \varepsilon_m^-; \vec{k}_{\parallel}\right) = -c_m^{-*}\tilde{\phi}\left(0, m; \vec{k}_{\parallel}\right) \approx 0, \; m = 3, 4. \tag{52}$$

Inter-band matrix element $P_{cv}(\vec{k}_{\parallel}, g)$ determined by formula (30) of [36]:

$$P_{cv}(\vec{k}_{\|},g)=\frac{1}{v_0}\int_{v_0} d\vec{\rho}U^{*}_{c,s,g}(\vec{\rho})e^{ik_y\rho_y}\frac{\partial}{\partial\rho_i}U_{v,p,i,g-k_x}(\vec{\rho}), \tag{53}$$

involves canonical momentum operator $\hat{P}=-i\hbar\vec{\nabla}$ and the periodic parts of the electron Bloch wave functions integrated on volume v_0 of the elementary lattice cell. The periodic part of the *s*-type conduction band is denoted as $U_{c,s,g}(\vec{\rho})$, whereas the periodic parts of the *p*-type valence band have structures $\left(U_{v,p,x,q}(\vec{\rho})\pm U_{v,p,y,q}(\vec{\rho})\right)/\sqrt{2}$ similar to expressions $(x\pm iy)/\sqrt{2}$ characterized by projections M of the orbital momentum on the magnetic field direction equal to ±1. For the c–v bands of different parities, as in the present case and in GaAs-type crystals, this matrix element in the zeroth approximation on the small wave vector $\vec{k}_{\|}$ and g is different from zero. It is considered to be of the allowed type in the definition of Elliott [43, 44] and is denoted as $P_{cv}(\vec{k}_{\|},g)\approx P_{cv}(0)$. The value of it cannot be changed by magnetic field strength. Even if this field is considered to be strong with the electron cyclotron energy greater than the exciton binding energy, nevertheless, this energy is much smaller than the semiconductor energy band gap E^0_g.

The two selected dipole-active magnetoexciton states F_1 and F_4 are characterized by coefficients $\varphi\left(F_1,B,\vec{k}\right)$ and $\varphi\left(F_4,B,\vec{k}\right)$ determining the magnetoexciton–photon interaction. They have the expressions

$$\varphi\left(F_1,B,\vec{k}\right)=\left(\frac{-e}{m_0l_0}\right)\sqrt{\frac{\hbar}{L_c\omega_{\vec{k}}}}P_{cv}\left(0\right)a_0^{-*}d_0^{-*},\quad \varphi\left(F_4,B,\vec{k}\right)=\left(\frac{e}{m_0l_0}\right)\sqrt{\frac{\hbar}{L_c\omega_{\vec{k}}}}P_{cv}\left(0\right), \tag{54}$$

where frequency $\omega_{\vec{k}}$ of the photon confined in the microcavity can be written in the form

$$\begin{gathered}\hbar\omega_{\vec{k}}=\frac{\hbar c}{n_c}\sqrt{\left(\frac{\pi}{L_c}\right)^2+\vec{k}_{\|}^2}\approx\hbar\omega_c+\frac{\hbar^2\vec{k}_{\|}^2}{2m_c}=\hbar\omega_c\left(1+\frac{x^2}{2}\right),\ x<1,\\ \vec{k}=\pm\frac{\pi}{L_c}\vec{a}_3+\vec{k}_{\|},\ \left|\vec{k}_{\|}\right|=x\frac{\pi}{L_c},\ \omega_c=\frac{c}{n_c}\frac{\pi}{L_c},\ \omega_cL_c=\frac{c\pi}{n_c},\ m_c=\frac{\hbar\pi n_c}{cL_c}.\end{gathered} \tag{55}$$

In the limit $x\to0$ the Rabi splitting energies are determined by the doubled absolute values of the interaction coefficients

$$\begin{gathered}\hbar\Omega_R(F_1,B)=2\left|\varphi(F_1,B,\pi/L_c)\right|=\frac{2e}{m_0l_0}\sqrt{\frac{\hbar n_c}{\pi c}}\left|P_{cv}(0)\right|\left|a_0^-\right|\left|d_0^-\right|,\\ \hbar\Omega_R(F_4,B)=2\left|\varphi(F_4,B,\pi/L_c)\right|=\frac{2e}{m_0l_0}\sqrt{\frac{\hbar n_c}{\pi c}}\left|P_{cv}(0)\right|.\end{gathered} \tag{56}$$

In this approximation, the Rabi splitting frequencies do not depend on cavity frequency ω_c or on cavity length L_c. They were estimated in [27] in the case of a GaAs-type QW with $\left|P_{cv}(0)\right|\approx2\cdot10^{-20}$ g·cm/sec. Their dependence on the magnetic field strength is determined by magnetic length l_0. The Rabi splitting increases with increasing magnetic field strength B as $\sqrt{B}$: $\hbar\Omega_R\sim\sqrt{B}$.

The creation energy of a magnetoexciton in state F_n and with wave vector $\vec{k}_{\|}$ is determined by formulas (46) and (49) and has the form

$$E_{mex}(F_n,\vec{k}_{\|}) = E_g^0 + E_e(R_i) + E_h(R_j) - I_{ex}(F_n,B,0) + \hbar^2\vec{k}_{\|}^2 \big/ 2M(F_n,B). \tag{57}$$

Introducing the energy detuning Δ between semiconductor energy band gap E_g^0 and cavity mode energy $\hbar\omega_c$ as $\Delta = \hbar\omega_c - E_g^0$ and using the dimensionless wave number x related with cavity length L_c as is shown in formula (55), expression (57) can be transcribed in the form:

$$\begin{gathered} E_{mex}(F_n,x) = \hbar\omega_c - \Delta + L(F_n,B) + \hbar g(F_n,B)\, x^2 \big/ 2, \\ L(F_n,B) = E_e(R_i) + E_h(R_j) - I_{ex}(F_n,B,0),\ \hbar g(F_n,B) = \hbar^2\pi^2 \big/ (M(F_n,B)L_c^2),\ x = \left|\vec{k}_{\|}\right| L_c \big/ \pi < 1. \end{gathered} \tag{58}$$

On the basis of expressions (54)–(58), the dispersion law of the cavity magnetoexciton polaritons can be written as follows [45, 46]:

$$\begin{aligned} E_{\substack{\mathrm{up}\\ \mathrm{lp}}} = \hbar\omega_c + \frac{1}{2}\Bigg[& -\Delta + L(F_n,B) + \hbar g(F_n,B)\frac{x^2}{2} + \hbar\omega_c\, x^2\big/2 \pm \\ & \pm\sqrt{\left(-\Delta + L(F_n,B) + \hbar g(F_n,B)\frac{x^2}{2} - \hbar\omega_c\frac{x^2}{2}\right)^2 + \left|\hbar\Omega_R(F_n,B)\right|^2}\,\Bigg]. \end{aligned} \tag{59}$$

Unlike [27], where Rabi energy $\hbar\omega_R = |\varphi(F_n,B)|$ was introduced, Rabi splitting energy $\hbar\Omega_R = 2\hbar\omega_R$ is used above following [45, 46]

Here, only one dipole-active magnetoexciton branch strongly interacting with the cavity photons with a given circular polarization was taken into account. In reality, there are two other quadrupole-active and another dipole-active magnetoexciton branches weakly interacting with the cavity photons with a given selected circular polarization. The more complicate picture of the polariton branches arising due to the interaction of four magnetoexciton branches with the cavity photons with a given circular polarization is discussed below.

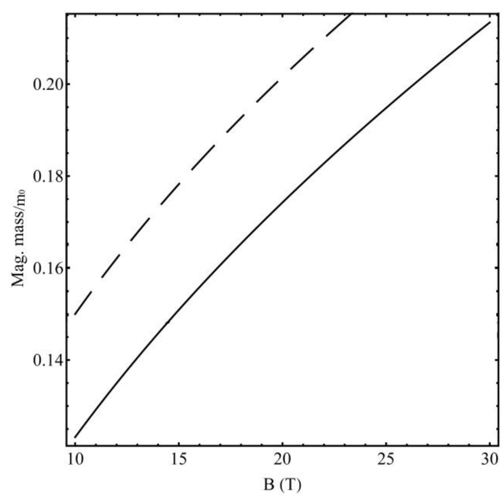

Fig. 8. Dependences of the magnetic masses in two dipole-active states F_1 (dashed line) and F_4 (solid line) on the magnetic field strength.

The zeroth-order Hamiltonian describing the free 2D magnetoexcitons, the cavity photons, and their interaction has a quadratic form and consists of three parts:

$$H_2 = H^0_{mex} + H^0_{ph} + H_{mex-ph}. \tag{60}$$

For simplicity, denotation (24) of the magnetoexciton creation operators will be shortened as follows:

$$\begin{aligned}
\psi^+_{ex}\left(F_1,\vec{k}_\parallel\right) &= \psi^+_{ex}\left(\vec{k}_\parallel, R_1, -1, \varepsilon^-_3\right)\\
\psi^+_{ex}\left(F_2,\vec{k}_\parallel\right) &= \psi^+_{ex}\left(\vec{k}_\parallel, R_2, -1, \varepsilon^-_3\right)\\
\psi^+_{ex}\left(F_3,\vec{k}_\parallel\right) &= \psi^+_{ex}\left(\vec{k}_\parallel, R_1, 1, \varepsilon_0\right)\\
\psi^+_{ex}\left(F_4,\vec{k}_\parallel\right) &= \psi^+_{ex}\left(\vec{k}_\parallel, R_2, 1, \varepsilon_0\right)\\
\psi^+_{ex}\left(F_5,\vec{k}_\parallel\right) &= \psi^+_{ex}\left(\vec{k}_\parallel, R_1, -1, \varepsilon^-_4\right)\\
\psi^+_{ex}\left(F_6,\vec{k}_\parallel\right) &= \psi^+_{ex}\left(\vec{k}_\parallel, R_2, -1, \varepsilon^-_4\right).
\end{aligned} \tag{61}$$

In Hamiltonian H_2, only dipole-active magnetoexciton states F_1 and F_4 and quadrupole-active states F_3 and F_5 were included:

$$H^0_{mex} = \sum_{n=1,3,4,5} E_{ex}\left(F_n,\vec{k}_\parallel\right)\psi^+_{ex}\left(F_n,\vec{k}_\parallel\right)\psi_{ex}\left(F_n,\vec{k}_\parallel\right). \tag{62}$$

The two remaining states F_2 and F_6 were excluded because they are forbidden in both approximations.

The cavity photons have wave vectors $\vec{k} = \vec{a}_3\vec{k}_z + \vec{k}_\parallel$ consisting of two parts. The longitudinal component is oriented along the axis of the resonator determined by unit vector $\vec{a}_3$ perpendicular to the surface of the QW embedded inside the microcavity. It has a fairly definite value of $k_z = \pm\pi/L_c$, where L_c is the cavity length. Transverse component $\vec{k}_\parallel = \vec{a}_1 k_x + \vec{a}_2 k_y$ is a 2D vector oriented in-plane of the QW; it is determined by two in-plane unit vectors $\vec{a}_1$ and $\vec{a}_2$. Vectors $\vec{\sigma}^\pm_{\vec{k}}$ of the light circular polarizations can be constructed introducing two unit vectors $\vec{s}$ and $\vec{t}$ perpendicular to light wave vector $\vec{k}$ and to each other as follows:

$$\begin{gathered}
\vec{\sigma}^\pm_{\vec{k}} = \frac{1}{\sqrt{2}}\left(\vec{s} \pm i\vec{t}\right);\ \vec{k} = \vec{a}_3 k_z + \vec{k}_\parallel;\ k_z = \pm\frac{\pi}{L_c};\ \vec{k}_\uparrow = \vec{a}_3\frac{\pi}{L_c} + \vec{k}_\parallel;\ \vec{k}_\downarrow = -\vec{a}_3\frac{\pi}{L_c} + \vec{k}_\parallel;\\
\vec{s} = \vec{a}_3\frac{\left|\vec{k}_\parallel\right|}{\left|\vec{k}\right|} - \frac{\vec{k}_\parallel \cdot k_z}{\left|\vec{k}\right|\left|\vec{k}_\parallel\right|};\ \vec{t} = \frac{\vec{a}_1 k_y - \vec{a}_2 k_x}{\left|\vec{k}_\parallel\right|};\ \left|\vec{k}_\uparrow\right| = \left|\vec{k}_\downarrow\right| = \left|\vec{k}\right|.
\end{gathered} \tag{63}$$

They obey the orthogonality and normalization conditions

$$\begin{gathered}
\left(\vec{k}\cdot\vec{t}\right) = \left(\vec{s}\cdot\vec{k}\right) = \left(\vec{t}\cdot\vec{s}\right) = 0;\ \left|\vec{s}\right| = \left|\vec{t}\right| = 1\\
\left(\vec{\sigma}^+_{\vec{k}}\right)^* = \vec{\sigma}^-_{\vec{k}};\ \left|\vec{\sigma}^\pm_{\vec{k}}\right| = 1\\
\left(\vec{\sigma}^\pm_{\vec{k}}\cdot\vec{\sigma}^{\mp^*}_{\vec{k}}\right) = 0;\ \left(\vec{\sigma}^\pm_{\vec{k}}\cdot\vec{\sigma}^{\pm^*}_{\vec{k}}\right) = 1
\end{gathered} \tag{64}$$

and have the form

$$\vec{\sigma}_{\vec{k}}^{\pm} = \frac{1}{\sqrt{2}\left|\vec{k}\right|\left|\vec{k}_{\parallel}\right|}\left\{\vec{a}_3\left|\vec{k}_{\parallel}\right|^2 + \vec{a}_1\left(-k_x k_z \pm i k_y\left|\vec{k}\right|\right) + \vec{a}_2\left(-k_y k_z \mp i k_x\left|\vec{k}\right|\right)\right\} = \left(\vec{\sigma}_{\vec{k}}^{\mp}\right)^*;$$
$$\vec{\sigma}_{\pm1} = \left(\vec{a}_1 \pm i\vec{a}_2\right)/\sqrt{2} = \vec{\sigma}_{\mp1}^*. \qquad (65)$$

Here, magnetoexciton circular polarization vectors $\vec{\sigma}_{\pm1}$ determined by formula (45) should be remembered. The required scalar products of the photon and magnetoexciton circular polarization vectors are listed below:

$$\left|\left(\vec{\sigma}_{\vec{k}}^{\pm}\cdot\vec{\sigma}_1^*\right)\right|^2 = \frac{1}{4\left|\vec{k}\right|^2}\left(k_z \pm \left|\vec{k}\right|\right)^2 \cong \frac{1}{2}\left(1 \pm \frac{k_z}{\left|k_z\right|}\right)\left(1 - \frac{x^2}{2} + \frac{x^4}{2}\right) \mp \frac{x^4}{16}\cdot\frac{k_z}{\left|k_z\right|};$$
$$\left|\left(\vec{\sigma}_{\vec{k}}^{\pm}\cdot\vec{\sigma}_{-1}^*\right)\right|^2 = \frac{1}{4\left|\vec{k}\right|^2}\left(k_z \mp \left|\vec{k}\right|\right)^2 \cong \frac{1}{2}\left(1 \mp \frac{k_z}{\left|k_z\right|}\right)\left(1 - \frac{x^2}{2} + \frac{x^4}{2}\right) \pm \frac{x^4}{16}\cdot\frac{k_z}{\left|k_z\right|}; \qquad (66)$$
$$\left|\vec{k}\right| = \sqrt{\left|k_z\right|^2 + \left|\vec{k}_{\parallel}\right|^2} = \left|k_z\right|\sqrt{1+x^2} \cong \left|k_z\right|\left(1 + \frac{x^2}{2} - \frac{x^4}{8}\right);\ x^2 = \frac{\left|\vec{k}_{\parallel}\right|^2 L_c^2}{\pi^2} < 1;\ k_z = \pm\frac{\pi}{L_c}.$$

Geometric rules (66) depend not only on the signs of circular polarization vectors $\vec{\sigma}_{\vec{k}}^{\pm}$, but also on the signs of projections k_z of photon wave vector $\vec{k}$. To take both details into account, new denotations of circular polarization vectors $\vec{\sigma}_{\vec{k}_{\uparrow}}^{\pm}$ and $\vec{\sigma}_{\vec{k}_{\downarrow}}^{\pm}$ are introduced. In these denotations, geometric selection rules (66) can be transcribed as follows:

$$\left|\left(\vec{\sigma}_{\vec{k}_{\uparrow}}^{+}\cdot\vec{\sigma}_1^*\right)\right|^2 = \left|\left(\vec{\sigma}_{\vec{k}_{\uparrow}}^{-}\cdot\vec{\sigma}_{-1}^*\right)\right|^2 = \left|\left(\vec{\sigma}_{\vec{k}_{\downarrow}}^{+}\cdot\vec{\sigma}_{-1}^*\right)\right|^2 = \left|\left(\vec{\sigma}_{\vec{k}_{\downarrow}}^{-}\cdot\vec{\sigma}_1^*\right)\right|^2 = \left(1 - \frac{x^2}{2} + \frac{7}{16}x^4\right), \qquad (67)$$
$$\left|\left(\vec{\sigma}_{\vec{k}_{\uparrow}}^{+}\cdot\vec{\sigma}_{-1}^*\right)\right|^2 = \left|\left(\vec{\sigma}_{\vec{k}_{\uparrow}}^{-}\cdot\vec{\sigma}_1^*\right)\right|^2 = \left|\left(\vec{\sigma}_{\vec{k}_{\downarrow}}^{+}\cdot\vec{\sigma}_1^*\right)\right|^2 = \left|\left(\vec{\sigma}_{\vec{k}_{\downarrow}}^{-}\cdot\vec{\sigma}_{-1}^*\right)\right|^2 = \frac{x^4}{16}.$$

The zeroth-order Hamiltonian of the cavity photons with wave vectors $\vec{k}$ and circular polarizations $\vec{\sigma}_{\vec{k}}^{\pm}$ described in (63) has the form

$$H_{ph}^0 = \sum_{\vec{k}_{\parallel}, k_z = \pm\pi/L_c} \hbar\omega_{\vec{k}}\left[\left(C_{\vec{k},+}\right)^+ C_{\vec{k},+} + \left(C_{\vec{k},-}\right)^+ C_{\vec{k},-}\right]. \qquad (68)$$

The creation and annihilation operators of the photons with circular polarizations $\vec{\sigma}_{\vec{k}}^{\pm}$ and with linear polarizations $\vec{s}$ and $\vec{t}$ are related as follows:

$$C_{\vec{k},\pm} = \frac{1}{\sqrt{2}}\left(C_{\vec{k},s} \pm iC_{\vec{k},t}\right),\ \left(C_{\vec{k},\pm}\right)^+ = \frac{1}{\sqrt{2}}\left(C_{\vec{k},s}^+ \mp iC_{\vec{k},t}^+\right),$$
$$\vec{s}C_{\vec{k},s} + \vec{t}C_{\vec{k},t} = C_{\vec{k},-}\vec{\sigma}_{\vec{k}}^{+} + C_{\vec{k},+}\vec{\sigma}_{\vec{k}}^{-},\quad \vec{s}C_{\vec{k},s}^+ + \vec{t}C_{\vec{k},t}^+ = \left(C_{\vec{k},-}\right)^+\vec{\sigma}_{\vec{k}}^{-} + \left(C_{\vec{k},+}\right)^+\vec{\sigma}_{\vec{k}}^{+}. \qquad (69)$$

The Hamiltonian describing the magnetoexciton–photon interaction including only the resonance terms and taking into account the two photon circular polarizations has the form

$$H_{mex-ph} = \sum_{\vec{k}_{\parallel}, k_z = \pm\pi/L_c}\left\{\varphi\left(F_1, \vec{k}_{\parallel}\right)\left[C_{\vec{k},-}\left(\vec{\sigma}_{\vec{k}}^{+}\cdot\vec{\sigma}_{-1}^*\right) + C_{\vec{k},+}\left(\vec{\sigma}_{\vec{k}}^{-}\cdot\vec{\sigma}_{-1}^*\right)\right]\psi_{ex}^{+}\left(F_1, F_{\parallel}\right) +\right.$$
$$+\varphi\left(F_4, \vec{k}_{\parallel}\right)\left[C_{\vec{k},-}\left(\vec{\sigma}_{\vec{k}}^{+}\cdot\vec{\sigma}_1^*\right) + C_{\vec{k},+}\left(\vec{\sigma}_{\vec{k}}^{-}\cdot\vec{\sigma}_1\right)\right]\psi_{ex}^{+}\left(F_4, \vec{k}_{\parallel}\right) +$$

$$+\varphi\left(F_3,\vec{k}_{\|}\right)\left[C_{\vec{k},-}\left(\vec{\sigma}_{\vec{k}}^{+}\cdot\vec{\sigma}_{1}^{*}\right)+C_{\vec{k},+}\left(\vec{\sigma}_{\vec{k}}^{-}\cdot\vec{\sigma}_{1}\right)\right]\psi_{ex}^{+}\left(F_3,\vec{k}_{\|}\right)+$$
$$+\varphi\left(F_5,\vec{k}_{\|}\right)\left[C_{\vec{k},-}\left(\vec{\sigma}_{\vec{k}}^{+}\cdot\vec{\sigma}_{-1}^{*}\right)+C_{\vec{k},+}\left(\vec{\sigma}_{\vec{k}}^{-}\cdot\vec{\sigma}_{-1}^{*}\right)\right]\psi_{ex}^{+}\left(F_5,\vec{k}_{\|}\right)+H.c.\}. \tag{70}$$

Coefficients $\varphi\left(F_n,\vec{k}_{\|}\right)$ and their square moduli are

$$\varphi\left(F_1,\vec{k}_{\|}\right)=-\phi_{cv}a_0^{-*}d_0^{-*};\ \left|\varphi\left(F_1,\vec{k}_{\|}\right)\right|^2=\left|\phi_{cv}\right|^2\left|a_0^{-}\right|^2\left|d_0^{-}\right|^2;$$
$$\varphi\left(F_4,\vec{k}_{\|}\right)=\phi_{cv};\ \left|\varphi\left(F_4,\vec{k}_{\|}\right)\right|^2=\left|\phi_{cv}\right|^2;$$
$$\varphi\left(F_3,\vec{k}_{\|}\right)=-\phi_{cv}b_1^{-*}(k_x+ik_y)l_0\big/\sqrt{2};\ \left|\varphi\left(F_3,\vec{k}_{\|}\right)\right|^2=\left|\phi_{cv}\right|^2\left|b_1^{-}\right|^2\left|\vec{k}_{\|}\right|^2l_0^2\big/2; \tag{71}$$
$$\varphi\left(F_5,\vec{k}_{\|}\right)=-\phi_{cv}a_0^{-*}d_0^{-*}(k_x+ik_y)l_0\big/\sqrt{2};\ \left|\varphi\left(F_5,\vec{k}_{\|}\right)\right|^2=\left|\phi_{cv}\right|^2\left|a_0^{-}\right|^2\left|d_0^{-}\right|^2\cdot\left|\vec{k}_{\|}\right|^2l_0^2\big/2;$$
$$\phi_{cv}=\frac{e}{m_0l_0}\sqrt{\frac{\hbar n_c}{\pi c}}P_{cv}(0);\ \left|\phi_{cv}\right|^2=\left(\frac{\hbar n_c}{\pi c}\right)\left|\frac{eP_{cv}(0)}{m_0l_0}\right|^2;\ f_{osc}=\left|\frac{\phi_{cv}}{\hbar\omega_c}\right|^2=\frac{\hbar n_c}{\pi c}\cdot\left|\frac{eP_{cv}(0)}{m_0l_0\hbar\omega_c}\right|^2.$$

Below, dimensionless value $f_{osc}=\left|\phi_{ev}/\hbar\omega_c\right|^2$ playing the role of the oscillator strength will be used. Looking at those expressions, one can observe that the probabilities of dipole-active quantum transitions in magnetoexciton states F_1 and F_4 determined by expressions $\left|\varphi\left(F_1,\vec{k}_{\|}\right)\right|^2$ and $\left|\varphi\left(F_4,\vec{k}_{\|}\right)\right|^2$ are proportional to $\left|\phi_{cv}\right|^2\approx l_0^{-2}\approx B$ and exhibit an increasing linear dependence on magnetic field strength *B*. Unlike them, the probabilities of the quadrupole-active quantum transitions in magnetoexciton states F_3 and F_5 are proportional to expression $\left|\phi_{cv}\right|^2 l_0^2$, which does not depend on magnetic field strength B at all.

The equations of motion for four magnetoexciton annihilation operators $\psi_{ex}\left(F_n,\vec{k}_{\|}\right)$ with $n=1,3,4,5$, as well as for similar photon operators $C_{\vec{k},\pm}$ under stationary conditions, are as follows:

$$i\hbar\frac{d}{dt}\psi_{ex}\left(F_n,\vec{k}_{\|}\right)=\left[\psi_{ex}\left(F_n,\vec{k}_{\|}\right),\hat{H}_2\right]=\hbar\omega\psi_{ex}\left(F_n,\vec{k}_{\|}\right)$$
$$i\hbar\frac{d}{dt}C_{\vec{k},\pm}=\left[C_{\vec{k},\pm},\hat{H}_2\right]=\hbar\omega C_{\vec{k},\pm}. \tag{72}$$

Their particular expressions are

$$\left(\hbar\omega-E_{ex}\left(F_i,\vec{k}_{\|}\right)\right)\psi_{ex}\left(F_i,\vec{k}_{\|}\right)=\left[C_{\vec{k},-}\left(\vec{\sigma}_{\vec{k}}^{+}\cdot\vec{\sigma}_{-1}^{*}\right)+C_{\vec{k},+}\left(\vec{\sigma}_{\vec{k}}^{-}\cdot\vec{\sigma}_{-1}^{*}\right)\right]\varphi\left(F_i,\vec{k}_{\|}\right),\ i=1,5$$
$$\left(\hbar\omega-E_{ex}\left(F_j,\vec{k}_{\|}\right)\right)\psi_{ex}\left(F_j,\vec{k}_{\|}\right)=\left[C_{\vec{k},-}\left(\vec{\sigma}_{\vec{k}}^{+}\cdot\vec{\sigma}_{1}^{*}\right)+C_{\vec{k},+}\left(\vec{\sigma}_{\vec{k}}^{-}\cdot\vec{\sigma}_{1}^{*}\right)\right]\varphi\left(F_j,\vec{k}_{\|}\right),\ j=3,4$$
$$\left(\hbar\omega-\hbar\omega_{\vec{k}}\right)C_{\vec{k},\pm}=\left(\vec{\sigma}_{\vec{k}}^{\pm}\cdot\vec{\sigma}_{-1}\right)\varphi^{*}\left(F_1,\vec{k}_{\|}\right)\psi_{ex}\left(F_1,\vec{k}_{\|}\right)+ \tag{73}$$
$$+\left(\vec{\sigma}_{\vec{k}}^{\pm}\cdot\vec{\sigma}_{1}\right)\varphi^{*}\left(F_4,\vec{k}_{\|}\right)\psi\left(F_4,\vec{k}_{\|}\right)+\left(\vec{\sigma}_{\vec{k}}^{\pm}\cdot\vec{\sigma}_{1}\right)\varphi^{*}\left(F_3,\vec{k}_{\|}\right)\psi_{ex}\left(F_3,\vec{k}_{\|}\right)+$$
$$+\left(\vec{\sigma}_{\vec{k}}^{\pm}\cdot\vec{\sigma}_{-1}\right)\varphi^{*}\left(F_5,\vec{k}_{\|}\right)\psi_{ex}\left(F_5,\vec{k}_{\|}\right).$$

Dipole-active state F_1 and quadrupole-active state F_5 can be preferentially excited by the light with the circular polarization $\vec{\sigma}_{\vec{k}}^{-}$ propagating with $k_z = \pi/L_c > 0$, whereas dipole-active state F_4 and quadrupole-active state F_3 mainly react to the light with circular polarization $\vec{\sigma}_{\vec{k}}^{+}$ propagating in the same direction with $k_z = \pi/L_c > 0$. In the case when Hamiltonians (68) and (70) contain photons only with one circular polarization—either $\vec{\sigma}_{\vec{k}}^{+}$ or $\vec{\sigma}_{\vec{k}}^{-}$—equations (73) give rise to the following relationships:

$$\begin{aligned} &\psi\left(F_i,\vec{k}_{\|}\right) = C_{\vec{k},\pm}\frac{\left(\vec{\sigma}_{\vec{k}}^{\mp}\cdot\vec{\sigma}_{-1}^{*}\right)\varphi\left(F_i,\vec{k}_{\|}\right)}{\hbar\omega - E_{ex}\left(F_i,\vec{k}_{\|}\right)}, \\ &i = 1,5 \\ &\psi\left(F_j,\vec{k}_{\|}\right) = C_{\vec{k},\pm}\frac{\left(\vec{\sigma}_{\vec{k}}^{\mp}\cdot\vec{\sigma}_{1}^{*}\right)\varphi\left(F_j,\vec{k}_{\|}\right)}{\hbar\omega - E_{ex}\left(F_j,\vec{k}_{\|}\right)}. \\ &j = 3,4 \end{aligned} \tag{74}$$

Substituting these relations into equations of motion (73) for photon operators $C_{\vec{k},\pm}$, we will find two dispersion equations describing five branches of the energy spectrum of two different systems. One of them concerns photons with circular polarization $\vec{\sigma}_{\vec{k}}^{-}$ propagating with $k_z = \pi/L_c > 0$ and exciting mostly magnetoexciton state F_1 as well as other states F_3, F_4, F_5 with smaller oscillator strengths. The second system consists of magnetoexcitons in the same four states F_1, F_3, F_4, F_5 existing in the frame of the microcavity fulfilled by the photons with circular polarization $\vec{\sigma}_{\vec{k}}^{+}$ propagating with $k_z = \pi/L_c > 0$. These fifth-order algebraic dispersion equations are

$$\begin{aligned} \left(\hbar\omega - \hbar\omega_{\vec{k}}\right) = &\frac{\left|\left(\vec{\sigma}_{\vec{k}}^{\mp}\cdot\vec{\sigma}_{-1}^{*}\right)\right|^2\left|\varphi\left(F_1\vec{k}_{\|}\right)\right|^2}{\hbar\omega - E_{ex}\left(F_1,\vec{k}_{\|}\right)} + \frac{\left|\left(\vec{\sigma}_{\vec{k}}^{\mp}\cdot\vec{\sigma}_{1}^{*}\right)\right|^2\left|\varphi\left(F_4,\vec{k}_{\|}\right)\right|^2}{\hbar\omega - E_{ex}\left(F_4,\vec{k}_{\|}\right)} + \\ &+\frac{\left|\left(\vec{\sigma}_{\vec{k}}^{\mp}\cdot\vec{\sigma}_{1}^{*}\right)\right|^2\left|\varphi\left(F_3\vec{k}_{\|}\right)\right|^2}{\hbar\omega - E_{ex}\left(F_3,\vec{k}_{\|}\right)} + \frac{\left|\left(\vec{\sigma}_{\vec{k}}^{\mp}\cdot\vec{\sigma}_{-1}^{*}\right)\right|^2\left|\varphi\left(F_5,\vec{k}_{\|}\right)\right|^2}{\hbar\omega - E_{ex}\left(F_5,\vec{k}_{\|}\right)}. \end{aligned} \tag{75}$$

They describe four magnetoexciton branches and one photon branch with a given circular polarization—either $\vec{\sigma}_{\vec{k}}^{-}$ or $\sigma_{\vec{k}}^{+}$—when the photons are propagating with $k_z = \pm\pi/L_c$.

Below, we will consider the case where cavity mode energy $\hbar\omega_c$ may be tuned to the energy of the selected magnetoexciton level, in the vicinity of which the maximal development of the polariton branches is expected. There are two dipole-active magnetoexciton energy levels F_1 and F_4 in different circular polarizations. Their energies are essentially changed as a function of magnetic field strength B and other parameters of the theory. To obtain the required detuning, cavity-mode energy $\hbar\omega_c$ should be changed adjusting it to new values of the selected magnetoexciton energy level.

It is useful to introduce dimensionless values and detunings Δ_1 and Δ_4 as follows:

$$\begin{gathered}\hbar\omega=\hbar\omega_c+E,\quad \hbar\omega/\hbar\omega_c=1+\varepsilon,\quad \varepsilon=E/\hbar\omega_c,\\ \Delta_n=\hbar\omega_c-E_{ex}(F_n,B,0),\quad \frac{\Delta_n}{\hbar\omega_c}=\delta_n=1-\frac{E_{ex}(F_n,B,0)}{\hbar\omega_c},\\ \hbar\omega_c=\frac{E_{ex}(F_n,B,0)}{1-\delta_n},\quad |\delta_n|<1,\\ \frac{\hbar\omega-E_{ex}(F_n,B,0)}{\hbar\omega_c}=\varepsilon+\delta_n,\quad n=1,4.\end{gathered}\tag{76}$$

In these denotations, dispersion equation (75) can be transcribed for two different cases. One of them concerns the cavity with the mode in resonance with magnetoexciton energy level $E_{ex}(F_1,B,0)$ with detuning δ_1, where the cavity photons have circular polarization $\vec{\sigma}^-_{\vec{k}_\uparrow}$ or $\vec{\sigma}^+_{\vec{k}_\downarrow}$ and interact mainly with the magnetoexcitons in state F_1 with circular polarization $\vec{\sigma}_{-1}$ and wave vectors $\vec{k}_\parallel$. These photons interact also with other magnetoexcitons, such as dipole-active state F_4, yet in opposite circular polarization $\vec{\sigma}_{+1}$, as well as with the quadrupole-active magnetoexcitons in states F_3 and F_5. The respective dispersion equation has the form:

$$\begin{aligned}\left(\varepsilon-\frac{x^2}{2}\right)=f_{osc}\cdot\Bigg\{&\frac{|a_0^-|^2|d_0^-|^2\left(1-\frac{x^2}{2}+\frac{7}{16}x^4\right)}{\left(\varepsilon+\delta_1-\frac{n_c^2\hbar\omega_c}{M(F_1,B)c^2}\cdot\frac{x^2}{2}\right)}+\\ &+\frac{x^4/16}{\left(\varepsilon+1-\frac{E_{ex}(F_4,B,0)}{E_{ex}(F_1,B,0)}(1-\delta_1)-\frac{n_c^2\hbar\omega_c}{M(F_4,B)c^2}\cdot\frac{x^2}{2}\right)}+\\ &+\frac{|b_1^-|^2(\pi l_0/L_c)^2(x^6/32)}{\left(\varepsilon+1-\frac{E_{ex}(F_3,B,0)}{E_{ex}(F_1,B,0)}(1-\delta_1)-\frac{n_c^2\hbar\omega_c}{M(F_3,B)c^2}\cdot\frac{x^2}{2}\right)}+\\ &+\frac{|a_0^-|^2|d_0^-|^2(\pi l_0/L_c)^2x^2(1-x^2/2+7x^4/16)/2}{\left(\varepsilon+1-\frac{E_{ex}(F_5,B)}{E_{ex}(F_1,B)}(1-\delta_1)-\frac{n_c^2\hbar\omega_c}{M(F_5,B)c^2}\cdot\frac{x^2}{2}\right)}\Bigg\}.\end{aligned}\tag{77}$$

The second case concerns the cavity mode in resonance with magnetoexciton energy level $E_{ex}(F_4,B,0)$ with detuning δ_4, where the cavity photon have circular polarization $\vec{\sigma}^+_{\vec{k}_\uparrow}$ or $\vec{\sigma}^-_{\vec{k}_\downarrow}$. They interact mainly with the magnetoexcitons in state F_4 with circular polarization $\vec{\sigma}_{+1}$. There are also weak interactions with the dipole-active magnetoexciton state F_1 with opposite circular polarization $\vec{\sigma}_{-1}$ as well as with the quadrupole-active magnetoexciton states F_3 and F_5 with circular polarizations $\vec{\sigma}_1$ and $\vec{\sigma}_{-1}$, respectively. The dispersion equation is as follows:

$$\left(\varepsilon-\frac{x^2}{2}\right)=f_{osc}\left\{\frac{\left(1-\frac{x^2}{2}+\frac{7}{16}x^4\right)}{\varepsilon+\delta_4-\frac{n_c^2\hbar\omega_c}{M\left(F_4,B\right)c^2}\cdot\frac{x^2}{2}}+\right.$$

$$+\frac{(x^4/16)\left|a_0^-\right|^2\left|d_0^-\right|^2}{\left(\varepsilon+1-\frac{E_{ex}\left(F_1,B,0\right)}{E_{ex}\left(F_4,B,0\right)}\left(1-\delta_4\right)-\frac{n_c^2\hbar\omega_c}{M\left(F_1,B\right)c^2}\frac{x^2}{2}\right)}+$$

$$+\frac{\left|b_1^-\right|^2\left(\frac{\pi l_0}{L_c}\right)^2\frac{x^2}{2}\left(1-\frac{x^2}{2}+\frac{7}{16}x^4\right)}{\left(\varepsilon+1-\frac{E_{ex}\left(F_3,B,0\right)}{E_{ex}\left(F_4,B,0\right)}\left(1-\delta_4\right)-\frac{n_c^2\hbar\omega_c}{M\left(F_3,B\right)c^2}\cdot\frac{x^2}{2}\right)}+$$

$$\left.+\frac{\left|a_0^-\right|^2\left|d_0^-\right|^2\left(\frac{\pi l_0}{L_c}\right)^2\frac{x^6}{32}}{\left(\varepsilon+1-\frac{E_{ex}\left(F_5,B,0\right)}{E_{ex}\left(F_4,B,0\right)}\left(1-\delta_4\right)-\frac{n_c^2\hbar\omega_c}{M\left(F_5,B\right)c^2}\cdot\frac{x^2}{2}\right)}\right\}. \tag{78}$$

In both equations (77) and (78), factor $\left(1-x^2/2+7x^4/16\right)$ expresses geometric selection rules (67) concerning the quantum transitions from the ground state of the crystal to magnetoexcitons states F_1 and F_4 with their circular polarizations $\vec{\sigma}_{-1}$ and $\vec{\sigma}_1$ excited under the action of the photons with circular polarizations $\vec{\sigma}^-_{\vec{k}_\uparrow}$ or $\vec{\sigma}^+_{\vec{k}_\downarrow}$ in one case and $\vec{\sigma}^+_{\vec{k}_\uparrow}$ or $\vec{\sigma}^-_{\vec{k}_\downarrow}$ in the other case, respectively. Factor $\left(1-x^2/2+7x^4/16\right)$ differs from unity due to nonzero in-plane components $\vec{k}_\parallel$ of photon wave vectors $\vec{k}=\pm\vec{a}_3\,\pi/L_c+\vec{k}_\parallel$. Factor $x^4/16$ appears when dipole-active states F_1 and F_4 with their circular polarizations $\vec{\sigma}_{-1}$ and $\vec{\sigma}_1$ are excited by the photons with the opposite circular polarizations, such as $\vec{\sigma}^+_{\vec{k}_\uparrow}$ or $\vec{\sigma}^-_{\vec{k}_\downarrow}$ in the case of state F_1 and such as $\vec{\sigma}^+_{\vec{k}_\downarrow}$ or $\vec{\sigma}^-_{\vec{k}_\uparrow}$ in the case of state F_4. Nonzero quantum transition probabilities are possible in this case only at the oblique incidence of the photons with $\vec{k}_\parallel\neq 0$ on the surface of the QW embedded into the microcavity.

In the case of strongly perpendicular incident light, these quantum transitions are forbidden. Factor $x^2/2$ has another origin related with the difference in one between the quantum numbers n_e and n_h of the LQ levels for electrons and holes, as evidenced by formulas (50) and (51).

The combinations of terms $\left(1-x^2/2+7x^4/16\right)$ and $x^4/16$ with factor $x^2/2$ give rise to factors $(x^2/2)\left(1-x^2/2+7x^4/16\right)$ and $x^6/32$. All of them appear in dispersion equations (77) and (78).

The energy spectrum of the cavity magnetoexciton–polaritons with the energy of the cavity mode tuned to magnetoexciton energy level $E_{ex}\left(F_1, B, 0\right)$ was obtained by solving the fifth-order dispersion equation (77) and is shown in Figs. 9–11. They concern the case of the cavity photons with circular polarizations $\vec{\sigma}^-_{\vec{k}_\uparrow}$ or $\vec{\sigma}^+_{\vec{k}_\downarrow}$, where the cavity mode energy $\hbar\omega_c$ was tuned to magnetoexciton energy level $E_{ex}\left(F_1, B, 0\right)$ as follows: $\hbar\omega_c = E_{ex}\left(F_1, B, 0\right)/\left(1-\delta_1\right)$ with dimensionless detuning $\delta_1 = -0.01$.

Two values of magnetic field strength B of 20 and 40 T were considered. Energies $\hbar\omega_c$ were different in these cases. The obtained pictures essentially depend on the RSOC arising under the action of an external electric field applied perpendicularly to the surface of the QW being parallel to the external magnetic field. In the case of the 2D hhs, the RSOC is characterized by third-order chirality terms in wave vector k components, which inevitably lead to the collapse of the semiconductor energy gap. To avoid it, a fourth-order term of the type $\left|\vec{k}\right|^4$ proportional to electric field strength with NP parameter C was introduced in the hh dispersion law. Figure 9 represents the absence of RSOC and corresponds to parameters $E_z = 0$ and $C = 0$. Figures 10 and 11 illustrate the presence of RSOC with electric field strength $E_z = 30\,\mathrm{kV/cm}$ and parameter C of 20 and 30, respectively. In the frame of each of these three cases, four versions were calculated. They are attributed to the two above mentioned values of magnetic field strength—20 and 40 T—and to two values of unknown hh g-factors $g_h = \pm 5$. The electron g factor was supposed to be $g_e = 1$. It is evident from Figs. 9–11 that the bare cavity photon branch is intersected by the bare magnetoexciton state F_1 branches. Only the interaction of the magnetoexciton with the cavity photons with selected circular polarization $\vec{\sigma}^-_\uparrow$ or $\vec{\sigma}^+_\downarrow$ gives rise to the well distinguishable polariton pictures. At other intersection points denoted as $\left(n-c\right)$ with $n = 3, 4, 5$ the magnetoexciton–photon interactions are very weak. The reconstructed polariton curves in the vicinities of these points are shown only qualitatively so as to help the eye. The real values of the splittings arising due to the anticrossings at these points are denoted as $\Delta\left(n-c\right)$. The coordinates of these intersection points $X\left(n-c\right)$ and $Y\left(n-c\right)$, along with the respective splittings, are mentioned in the captions.

Forbidden bare magnetoexciton branches F_2 and F_6 are also shown in the figures because their presence will affect the kinetic and quantum statistic properties of high-density cavity magnetoexciton–polaritons. The description of other energy spectra in general outline is the same. However, the positions of the different magnetoexciton energy branches on the energy scale essentially depend on the full set of parameters $\left\{B, E_z, g_e, g_h, C\right\}$ which is demonstrated in Figs. 9–11.

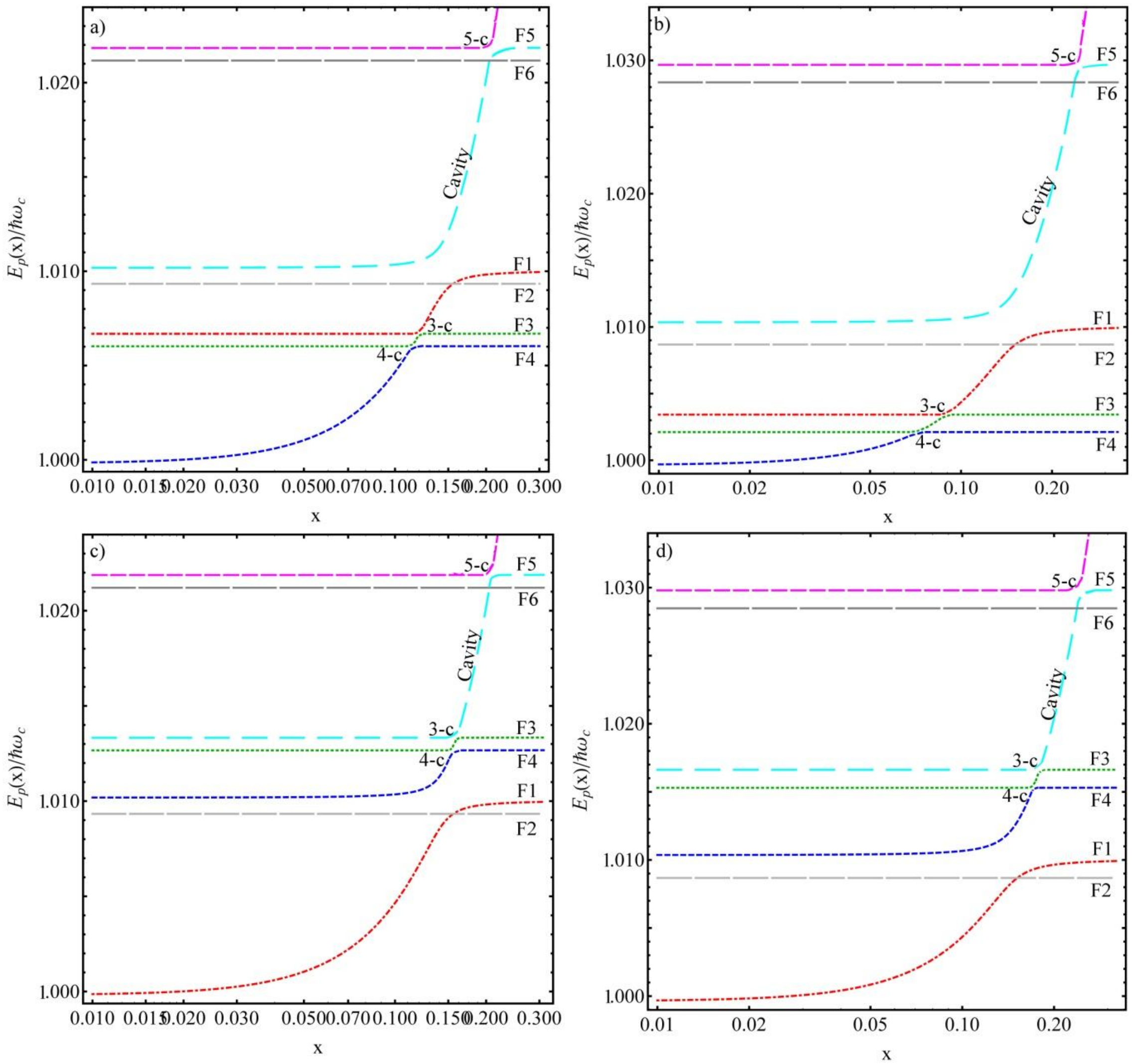

Fig. 9. Five cavity magnetoexciton–polariton energy branches as a function of dimensionless in-plane wave number x arising as a result of the interaction of the cavity photons with circular polarizations $\vec{\sigma}^{-}_{\vec{k}_\uparrow}$ or $\vec{\sigma}^{+}_{\vec{k}_\downarrow}$ with four magnetoexciton energy branches F_1, F_4, F_3 and F_5 characterized by circular polarizations $\vec{\sigma}_{\pm 1}$, two branches being dipole-active and two quadrupole active, where the cavity mode energy is tuned to magnetoexciton energy level $E_{ex}(F_1, B, 0)$. The case of the absence of an external electric field and RSOC with parameters $E_z = 0$ and $C = 0$ is represented in four versions. They appear from the combinations of two values of magnetic field strength B and two values of hh *g*-factor g_h as follows: (a) $B = 20\,\mathrm{T}$, $g_h = 5$; (b) $B = 40\,\mathrm{T}$, $g_h = 5$; (c) $B = 20\,\mathrm{T}$, $g_h = -5$; and (d) $B = 40\,\mathrm{T}$, $g_h = -5$. The electron *g*-factor was selected $g_e = 1$. For completeness, two forbidden magnetoexciton energy branches F_2 and F_6 are added. The intersection points and the splittings of the polariton curves at these points are as follows: (a) X_a(4-c) = 0.113; Y_a(4-c) = 1.00601; Δ_a(4-c) = $8.44 \cdot 10^{-6}$. X_a(3-c) = 0.120; Y_a(3-c) = 1.00670; Δ_a(3-c) = $8.46 \cdot 10^{-6}$. X_a(5-c) = 0.209; Y_a(5-c) = 1.02184; Δ_a(5-c) = $8.44 \cdot 10^{-6}$. (b) X_b(4-c) = 0.071; Y_b(4-c) = 1.00206; Δ_b(4-c) = $7.26 \cdot 10^{-6}$. X_b(3-c) = 0.089; Y_b(3-c) = 1.00338; Δ_b(3-c) = $7.31 \cdot 10^{-6}$. X_b(5-c) = 0.243; Y_b(5-c) = 1.02969; Δ_b(5-c) = $7.28 \cdot 10^{-6}$. (c) X_c(4-c) = 0.156; Y_c(4-c) = 1.01265; Δ_c(4-c) = $8.41 \cdot 10^{-6}$. X_c(3-c) = 0.160; Y_c(3-c) = 1.01333; Δ_c(3-c) = $8.44 \cdot 10^{-6}$. X_c(5-c) = 0.208; Y_c(5-c) = 1.02190; Δ_c(5-c) = $8.41 \cdot 10^{-6}$. and (d) X_d(4-c) = 0.171; Y_d(4-c) = 1.01529; Δ_d(4-c) = $5.94 \cdot 10^{-6}$. X_d(3-c) = 0.179; Y_d(3-c) = 1.01660; Δ_d(3-c) = $6.00 \cdot 10^{-6}$. X_d(5-c) = 0.243; Y_d(5-c) = 1.02976; Δ_d(5-c) = $5.96 \cdot 10^{-6}$.

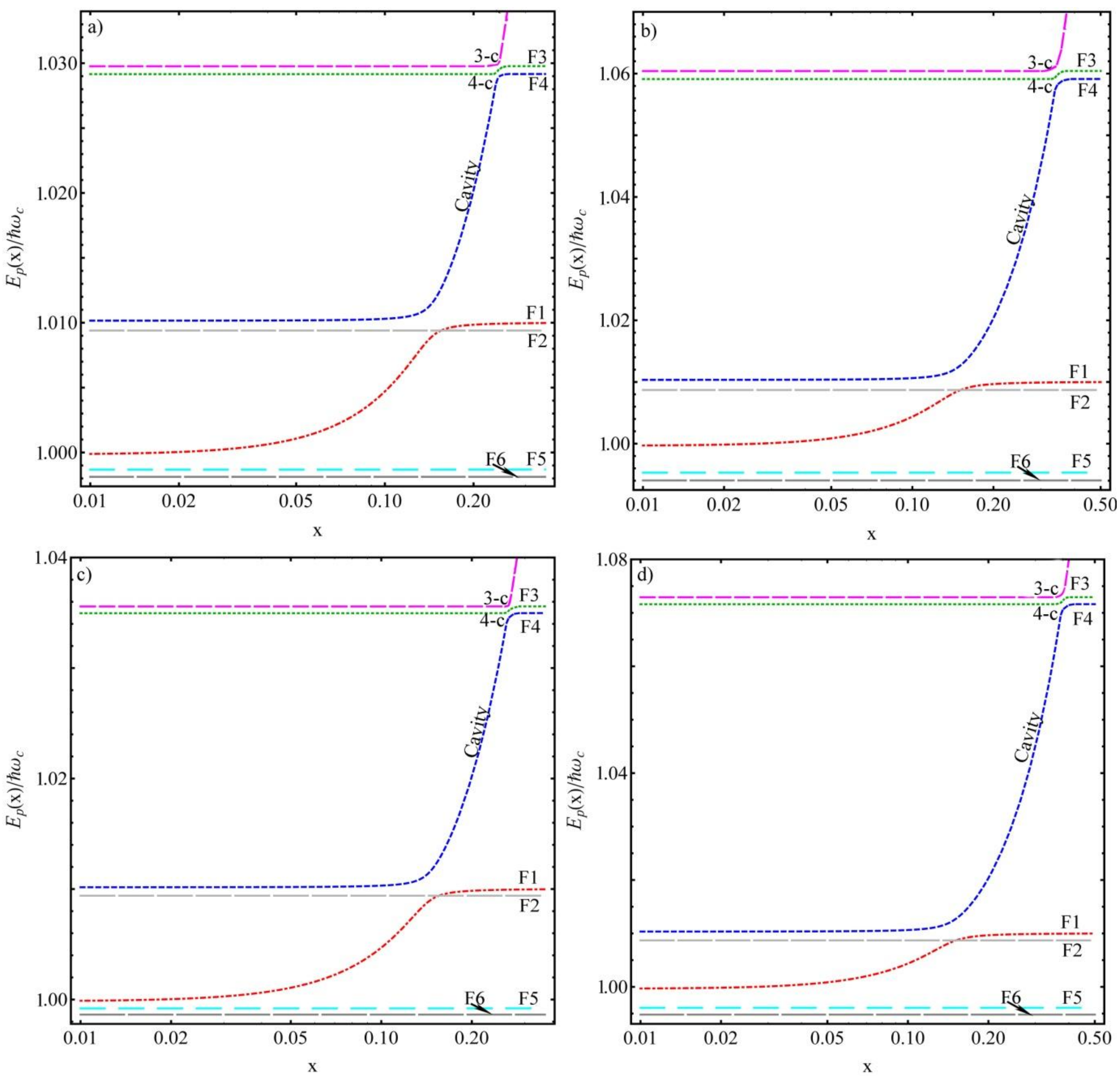

Fig. 10. Five cavity magnetoexciton–polariton energy branches as a function of dimensionless in-plane wave number x arising as result of the interaction of the cavity photons with circular polarizations $\vec{\sigma}^{-}_{\vec{k}_\uparrow}$ or $\vec{\sigma}^{+}_{\vec{k}_\downarrow}$ with four magnetoexciton energy branches F_1, F_4, F_3, and F_5 characterized by circular polarizations $\vec{\sigma}_{\pm 1}$, two branches being dipole-active and two quadrupole active, where the cavity mode energy is tuned to magnetoexciton energy level $E_{ex}(F_1, B, 0)$. The action of an external electric field and RSOC with parameters $E_z = 30$ kV/cm and $C = 20$ is represented in four versions. They appear from the combinations of two values of magnetic field strength B and two values of hh *g*-factor g_h as follows: (a) $B = 20$ T, $g_h = 5$; (b) $B = 40$ T, $g_h = 5$; (c) $B = 20$ T, $g_h = -5$; and (d) $B = 40$ T, $g_h = -5$. The electron *g*-factor was selected $g_e = 1$. For completeness, two forbidden magnetoexciton energy branches F_2 and F_6 are added. The intersection points and the splittings of the polariton curves at these points are as follows: (a) X(1-c) = 0.145; Y(1-c) = 1.01015. X_a(4-c) = 0.241; Y_a(4-c) = 1.02919; Δ_a(4-c) = 11.23 · 10^{-6}. X_a(3-c) = 0.245; Y_a(3-c) = 1.02980; Δ_a(3-c) = 11.29 · 10^{-6}. (b) X_b(4-c) = 0.343; Y_b(4-c) = 1.05920; Δ_b(4-c) = 15.74 · 10^{-6}. X_b(3-c) = 0.347; Y_b(3-c) = 1.06040; Δ_b(3-c) = 16 · 10^{-6}. (c) X_c(4-c) = 0.264; Y_c(4-c) = 1.03492; Δ_c(4-c) = 11.19 · 10^{-6}. X_c(3-c) = 0.268; Y_c(3-c) = 1.03561; Δ_c(3-c) = 11.26 · 10^{-6}. and (d) X_d(4-c) = 0.377; Y_d(4-c) = 1.07161; Δ_d(4-c) = 15.60 · 10^{-6}. X_d(3-c) = 0.380; Y_d(3-c) = 1.07287; Δ_d(3-c) = 15.91 · 10^{-6}.

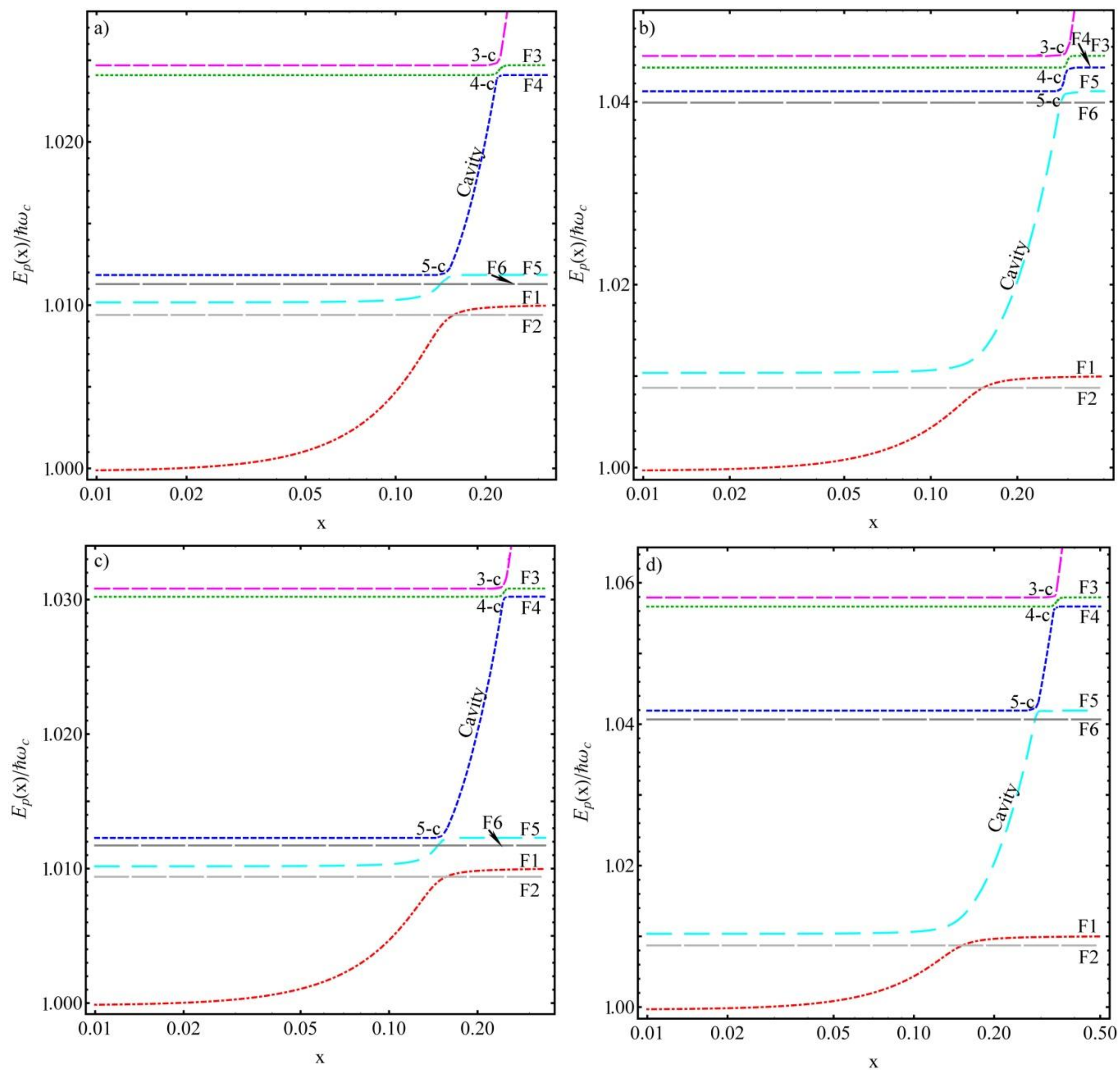

Fig. 11. Five cavity magnetoexciton–polariton energy branches as a function of dimensionless in-plane wave number x arising as result of the interaction of the cavity photons with circular polarizations $\vec{\sigma}^{-}_{\vec{k}_{\uparrow}}$ or $\vec{\sigma}^{+}_{\vec{k}_{\downarrow}}$ with four magnetoexciton energy branches F_1, F_4, F_3, and F_5 characterized by circular polarizations $\vec{\sigma}_{\pm 1}$, two branches being dipole-active and two quadrupole active, where the cavity mode energy is tuned to magnetoexciton energy level $E_{ex}\left(F_1, B, 0\right)$. The action of an external electric field and RSOC with parameters $E_z = 30\,\mathrm{kV/cm}$ and $C = 30$ is represented in four versions. They appear from the combinations of two values of magnetic field strength B and two values of hh *g*-factor g_h as follows: (a) $B = 20\,\mathrm{T}$, $g_h = 5$; (b) $B = 40\,\mathrm{T}$, $g_h = 5$; (c) $B = 20\,\mathrm{T}$, $g_h = -5$; and (d) $B = 40\,\mathrm{T}$, $g_h = -5$. The electron *g*-factor was selected $g_e = 1$. For completeness, two forbidden magnetoexciton energy branches F_2 and F_6 are added. The intersection points and the splittings of the polariton curves at these points are as follows: (a) X_a(5-c) = 0.148; Y_a(5-c) = 1.01182; Δ_a(5-c) = $9.47 \cdot 10^{-6}$. X_a(4-c) = 0.218; Y_a(4-c) = 1.02409; Δ_a(4-c) = $9.44 \cdot 10^{-6}$. X_a(3-c) = 0.222; Y_a(3-c) = 1.02470; Δ_a(3-c) = $9.49 \cdot 10^{-6}$. (b) X_b(5-c) = 0.285; Y_b(5-c) = 1.04116; Δ_b(5-c) = $10.39 \cdot 10^{-6}$. X_b(4-c) = 0.295; Y_b(4-c) = 1.04371; Δ_b(4-c) = $10.24 \cdot 10^{-6}$. X_b(3-c) = 0.300; Y_b(3-c) = 1.04502; Δ_b(3-c) = $10.41 \cdot 10^{-6}$. (c) X_c(5-c) = 0.151; Y_c(5-c) = 1.01227; Δ_c(5-c) = $10.67 \cdot 10^{-6}$. X_c(4-c) = 0.247; Y_c(4-c) = 1.03021; Δ_c(4-c) = $10.62 \cdot 10^{-6}$. X_c(3-c) = 0.249; Y_c(3-c) = 1.03081; Δ_c(3-c) = $10.68 \cdot 10^{-6}$. and (d) X_d(5-c) = 0.288; Y_d(5-c) = 1.04190; Δ_d(5-c) = $16.16 \cdot 10^{-6}$. X_d(4-c) = 0.336; Y_d(4-c) = 1.05672; Δ_d(4-c) = $15.96 \cdot 10^{-6}$. X_d(3-c) = 0.341; Y_d(3-c) = 1.05799; Δ_d(3-c) = $16.18 \cdot 10^{-6}$.

The energy spectra represented in Fig. 9 from one side and in Figs. 10, 11 from another one reveal the effect of the RSOC and the nonlinearity of the hh dispersion law leading to an essential and nonmonotonous displacement of the magnetoexciton energy branches on the energy scale. It makes it possible to introduce required changes in the energy spectra by slowly varying the external magnetic and electric fields.

5. Conclusions

The properties of 2D electrons, holes, magnetoexcitons, and cavity polaritons subjected to the action of strong perpendicular magnetic and electric fields have been reviewed and studied. To this end, exact solutions of the LQ of the 2D hhs accompanied by the RSOC with third-order chirality terms, by the ZS effects, and by the NP of their dispersion laws have been obtained [40] and examined additionally following the method proposed by Rashba [1]. His results concerning the conduction electrons have been supplemented taking into account the ZS effects. Using the mentioned wave functions for 2D electrons and holes, the Hamiltonians describing the Coulomb electron–electron and the electron–radiation interactions in the second quantization representation have been deduced [40]. In turn, the electron–radiation interaction Hamiltonian has made it possible to construct another Hamiltonian describing the magnetoexciton–photon interaction and to begin the development of the theory of magnetoexciton–polaritons. To do this, the wave functions of the 2D magnetoexcitons are needed. The six magnetoexciton states arising due to the composition of two LLLs for conduction electrons with three LLLs for hhs have been taken into consideration. Among them, two states—F_1 and F_4—are dipole-active, other two—F_3 and F_5—are quadrupole-active, and the last two—F_2 and F_6—are forbidden in the inter-band optical quantum transitions as well as in transitions from the ground state of the crystal to the magnetoexciton states in GaAs-type QWs. The dispersion equation describing the magnetoexciton–polariton energy spectrum includes the first four states F_1, F_3, F_4, and F_5 interacting with cavity photons in the two mentioned approximations. These four magnetoexciton degrees of freedom, together with the branch of the cavity photons, give rise to fifth-order dispersion equation with five polariton-type renormalized energy branches.

The obtained picture has been completed by adding two magnetoexciton energy-branches F_2 and F_6 forbidden in the optical quantum transitions. The cavity polariton energy spectrum essentially depends on the detuning between cavity mode energy $\hbar\omega_c$ and the energy of the magnetoexciton level as well as on the electron and hole g-factors. One version of this detuning has been studied [40] and discussed in the review. It concerns the detuning with energy level $E_{ex}(F_1,B,0)$ of dipole-active state F_1 with circular polarization $\vec{\sigma}_{-1}$ interacting with the cavity photons with circular polarization $\vec{\sigma}^-_{\vec{k}_\uparrow}$ or $\vec{\sigma}^+_{\vec{k}_\downarrow}$ propagating inside the microcavity with wave vectors $\vec{k}=\pm\vec{a}_3\,\pi/L_c+\vec{k}_\parallel$, respectively. The cavity mode energy was chosen to be $\hbar\omega_c\left(B\right)=E_{ex}(F_1,B,0)/(1-\delta_1)$ with dimensionless detuning $\delta_1=-0{,}01$. The $\hbar\omega_c(B)$ value varies as a function of magnetic field strength B and other parameters of the theory simultaneously with a change in magnetoexciton level energy $E_{ex}(F_1,B,0)$.

It has been found that two different signs $\pm$ of quantized component k_z of wave vector $\vec{k}$ are very important, giving rise to the gyrotropy effect. It consists in the dependence of the polariton energy spectrum on the photon propagation direction. It is determined by wave vector $\vec{k}_{\uparrow}$ with $k_z = \pi/L_c$ in one case and by wave vector $\vec{k}_{\downarrow}$ with $k_z = -\pi/L_c$ in the other case.

References

[1] E. I. Rashba, Fiz. Tverd. Tela 2, 1224, (1960) [Sov. Phys. Solid State 2, 1109, (1960)].
[2] W. Bardyszewski and S.P. Lepkowski, Phys. Rev. B 90, 075302, (2014).
[3] W. Bardyszewski and S.P. Lepkowski, Phys. Rev. B 85, 035318, (2012).
[4] M. Sobol and W. Bardyszewski, Phys. Rev. B 73, 075208, (2006).
[5] W. E. Lamb-Jr., Phys. Rev. 85, 259, (1952).
[6] S. A. Moskalenko, I. V. Podlesny, P. I. Khadzhi, B. V. Novikov, and A. A. Kiselyov, Solid State Commun. 151, 1690, (2011).
[7] S. A. Moskalenko, I. V. Podlesny, E. V. Dumanov, M. A. Liberman, and B. V. Novikov, Phys. Status Solidi B 252 (4), 730–742, (2015), DOI: 10.1002/pssb.201451296.
[8] D. Paquet, T. M. Rice, and K. Ueda, Phys. Rev. B 32, 5208 (1985).
[9] S. A. Moskalenko, M. A. Liberman, D. W. Snoke, and V. V. Botan, Phys. Rev. B 66, 245316, (2002).
[10] M. J. Snelling, E. Blackwood, C. J. McDonagh, R. T. Harley, and C. T. B. Foxon, Phys. Rev. B 45, 3922(R), (1992).
[11] P. Le Jeune, D. Robart, X. Mariey, T. Amandy, M. Brousseauy, J. Barrauy, V. Kalevichz, and D. Rodichev, Semicond. Sci. Technol. 12, 380–383, (1997).
[12] E. L. Ivchenko and A. A. Kiselev, Sov. Phys. Semicond. 26 (8), 1471 (1992).
[13] I. V. Soldatov et al., Physica E 57, 193, (2014).
[14] G. M. Minkov, A. A. Sherstobitov, A. V. Germanenko, O. E. Rut, V. A. Larionova, and B. N. Zvonkov, Phys. Rev. B 72, 165325, (2005).
[15] T. S. Shamirzaev, J. Debus, D. R. Yakovlev, M. M. Glazov, E. L. Ivchenko, and M. Bayer, Phys. Rev. B 94, 045411, (2016).
[16] I. A. Yugova, A. Greilich, D. R. Yakovlev, A. A. Kiselev, M. Bayer, V. V. Petrov, Yu. K. Dolgikh, D. Reuter, and A. D. Wieck, Phys. Rev. B 75, 245302, (2007).
[17] J. Debus, T. S. Shamirzaev, D. Dunker, V. F. Sapega, E. L. Ivchenko, D. R. Yakovlev, A. I. Toropov, and M. Bayer, Phys. Rev. B 90, 125431, (2014).
[18] G. E. Pikus and F. G. Pikus, Solid State Commun. 89, 319, (1994).
[19] A. A. Kiselev and L. V. Moiseev, Phys. Solid State 38, 866, (1996).
[20] D. M. Hofmann, K. Oettinger, Al. L. Efros, and B. K. Meyer, Phys. Rev. B 55, 9924, (1997).
[21] D. D. Solnyshkov, I. A. Shelykh, A. V. Kavokin, E. L. Ivchenko, and G. Malpuech, Phys. Rev. B 78 (16), 165323, (2008).
[22] I. A. Shelykh, A. V. Kavokin, and G. Malpuech, Phys. Status Solidi B 242 (11), 2271, (2005).
[23] Y. G. Rubo, A. V. Kavokin, and I. A. Shelykh, Phys. Lett. A 358 (3), 227-230, (2006).
[24] A. V. Larionov, V. D. Kulakovskii, S. Höfling, C. Schneider, L. Worschech, and A. Forchel, Phys. Rev. Lett. 105 (25), 256401, (2010).
[25] P. Walker, T. C. H. Liew, D. Sarkar, M. Durska, A.P.D. Love, M.S. Skolnick, J.S. Roberts, I. A. Shelykh, A. V. Kavokin, and D. N. Krizhanovskii, Phys. Rev. Lett. 106 (25), 257401, (2011).
[26] B. Pietka et al., Phys. Rev. B 91, 075309, (2015).
[27] S. A. Moskalenko, I. V. Podlesny, M. A. Liberman, and B. V. Novikov, J. Nanophotonics 6, 061806, (2012).

[28] V. D. Kulakovskii, A. S. Brichkin, S. V. Novikov, C. Schneider, S. Hofling, M. Kamp, A. Forchel, and N.A. Gippius, Phys. Rev. B 85, 155322, (2012).
[29] A. Rahimi-Iman, C. Schneider, J. Fischer, S. Holzinger, M. Amthor, S. Höfling, and S. Reitzenstein, Phys. Rev. B 84, 165325, (2014).
[30] T. T. Hopfield, Phys. Rev. 112, 1555, (1958).
[31] O. L. Berman, R. Y. Kezerashvili, and Y. E. Lozovik, Phys. Rev. B 80 (11), 115302, (2009).
[32] D. R. Yakovlev, V. P. Kochereshko, R. A. Suris, H. Schenk, W. Ossau, A. Waag, G. Landwehr, P. C. M. Christianen, and J.C. Maan, Phys. Rev. Lett. 79, 3974, (1997).
[33] S. A. Moskalenko, M. A. Liberman and I. V. Podlesny, Phys. Rev. B 79 (12), 125425, (2009).
[34] T. Hakioglu, M. A. Liberman, S. A. Moskalenko, and I. V. Podlesny, J. Phys.: Cond. Matt. 23, 345405, (2011).
[35] I. V. Podlesny, S. A. Moskalenko, T. Hakioglu, A. A. Kiselyov, and L. E. Gherciu, Physica E 49, 44, (2013).
[36] S. A. Moskalenko, I. V. Podlesny, E. V. Dumanov, and A. A. Kiselyov, J. Nanoelectron. Optoelectron. 9 (2), 219, (2014).
[37] R. Winkler, Spin-Orbit Coupling Effects in Two-Dimensional Electron and Hole Systems, Berlin, Springer Tracts in Modern Physics, vol. 191, 2003, 236 pages.
[38] T. Hakioglu and M. S. Sahin, Phys. Rev. Lett. 98, 166405, (2007).
[39] S. A. Moskalenko, E. V. Dumanov, I. V. Podlesny, M. A. Liberman, B. V. Novikov, S. S. Rusu, and V. M. Bajireanu, Mold. J. Phys. Sci. 13 (1-2), 61, (2014).
[40] S. A. Moskalenko, I. V. Podlesny, E. V. Dumanov, and M. A. Liberman, Eur. Phys. J. B 88, 218, (2015).
[41] E. V. Dumanov, I. V. Podlesny, S. A. Moskalenko, and M. A. Liberman, Physica E 88, 77, (2017).
[42] F. Meier and B. P. Zakharchenya, *ed*., Optical Orientation, Modern Problems in Condensed Matter Sciences, Amsterdam: North-Holland, vol. 8, 1984, 536 pages.
[43] R. J. Elliot, Phys. Rev. 108, 1384, (1957).
[44] S. A. Moskalenko, Vvedenie v teoriyu eksitonov bol'shoi plotnosti, Stiinta, Kishinev, 1983, 214 pages.
[45] H. Deng, H. Haug, and Y. Yamamoto, Rev. Mod. Phys. 82, 1489, (2010).
[46] J. Keeling, F. M. Marchetti, M. H. Szymanska, and P. B. Littlewood, Semicond. Sci. Technol. 22, R1, (2007).